The proliferation and differentiation programs are only partially coupled during *C. elegans* intestine development

Authors:

Joris Dieng[1], Grégoire Michaux[1,*], Anne Pacquelet[1,*]

[*] Corresponding authors

Affiliations :

[1] Univ Rennes, CNRS, IGDR (Institut de Génétique et de Développement de Rennes), UMR 6290, F-35000 Rennes, France

Contact information:

anne.pacquelet@univ-rennes1.fr

CNRS UMR6290 - IGDR
2 avenue du Professeur Léon Bernard
35043 Rennes Cedex
France

gregoire.michaux@univ-rennes1.fr

CNRS UMR6290 - IGDR
2 avenue du Professeur Léon Bernard
35043 Rennes Cedex
France

Abstract

Cell proliferation and differentiation are essential processes underlying multicellular organism development. Cell proliferation arrest usually precedes terminal differentiation, suggesting that these two processes may be coordinated. Here we took advantage of the very stereotyped development of the *C. elegans* intestine to address whether the control of the proliferation and differentiation programs are systematically coupled. We show that retarding cell cycle arrest leads to a delay in the recruitment of some, but not all, brush border components. Reciprocally, we find that cell cycle arrest relies on the differentiation factors ELT-2 and ELT-7 only in posterior intestinal cells. The occurrence of supernumerary divisions in the absence of ELT-2 and ELT-7 is associated with changes in the expression pattern of the cell cycle regulators CKI-1 and cyclin B1. Our work thus demonstrates the existence of reciprocal interactions between cell proliferation and cell differentiation. It nevertheless also shows that these two processes are only partially coupled, suggesting the existence of additional mechanisms ensuring their temporal control.

Introduction

The development of a single-cell egg into a multicellular organism involves both the generation of a large number of cells through cell proliferation and the acquisition of specialized cell functions through differentiation. Cell proliferation arrest usually precedes terminal differentiation, suggesting the existence of mechanisms that coordinate the two processes. Consistently, several mechanisms through which cell cycle regulators control the activity of differentiation factors have been described. Reciprocally, differentiation factors have been shown to induce the expression cell cycle inhibitors (Ruijtenberg and van den Heuvel, 2016). The inverse correlation between proliferation and differentiation has also led to the common hypothesis that cell cycle exit may be a prerequisite to differentiation. Although this is indeed the case in some instances (e.g. (Willms et al., 2020)), the situation appears to be more complex than anticipated and some examples of uncoupling between cell cycle exit and differentiation have been described (Cockburn et al., 2022; Lobjois et al., 2008;

Martinez et al., 2024). We therefore decided to investigate further how changes in cell proliferation affect differentiation during development and, reciprocally, how differentiation contributes to cell cycle regulation.

To address this question, we took advantage of the extremely stereotyped and well characterized development of the *C. elegans* intestine. This simple intestine is composed of 20 cells, which all derive from a single embryonic precursor cell, the E blastomere. This blastomere undergoes a series of cell divisions that successively give rise to the so-called E2, E4, E8, E16 and E20 intestinal development stages (Fig.S1) (Asan et al., 2016; Leung et al., 1999; Sulston et al., 1983). First, the E blastomere and all its descendants divide four times to produce 16 intestinal cells, which are organized into eight intestinal rings, each being formed by two cells (Fig.S1). Cells from the first and last intestinal rings then divide once more, thereby giving rise to the 20-cell stage intestine, formed by nine intestinal rings, all containing 2 cells, except the first anterior ring which is constituted by 4 cells (Fig.S1) (Asan et al., 2016).

While all early embryonic divisions are characterized by a quick succession of S and M phases, cell cycle length progressively increases in the E lineage from the E2 stage on until it becomes markedly long between the E16 and E20 stage (Leung et al., 1999; Sulston et al., 1983). The initial increase in intestinal cell cycle length is due to the introduction of a G2 phase at the E2 stage while a G1 phase is probably introduced only at the E16 stage (Edgar and McGhee, 1988; Wong et al., 2022). The CDC-25.1 phosphatase, which promotes G2/M transition through the activation of the cyclin dependent kinase CDK-1, has been shown to be required for intestinal divisions and embryos carrying *cdc-25.1* gain-of-function mutations present an acceleration of intestinal divisions (Bao et al., 2008; Clucas et al., 2002; Demouchy et al., 2024; Kostić and Roy, 2002). The CDC-25-2 phosphatase also appears to regulate intestinal divisions: in *cdc-25-2* loss-of-function mutants, the E2 to E4 division has been reported to be slower and the E16 to E20 division does not occur, suggesting that CDC-25-2 contributes to cell cycle progression together with CDC-25.1 in early intestinal divisions and becomes essential for the E16 to E20 division (Lee et al., 2016; Nair et al., 2013). On the other hand, the WEE-1.1 kinase starts to be

expressed in the intestinal lineage at the E2 stage and prevents G2/M transition through the inhibition of CDK-1, thereby contributing to cell cycle length increase (Robertson et al., 2014). Consistent with the late appearance of a G1 phase, cyclin D1 (CYD-1), which promotes G1 progression, is required solely for the E16 to E20 division (Boxem and Van Den Heuvel, 2001). Loss of the CDK inhibitor CKI-1 also does not affect cell cycle length until the E16 stage but leads to the abnormal late division of all intestinal cells after the E16 stage (Kostić and Roy, 2002). Altogether, those observations suggest that both CYD-1 and CKI-1 are essential regulators of the E16 to E20 division, with CYD-1 promoting G1 progression and division in the most anterior and posterior intestinal cells and CKI-1 preventing cell cycle progression in the remaining enterocytes.

Intestinal fate specification relies on the restricted expression of two GATA transcription factors, END-1 and END-3, in the E blastomere (Maduro et al., 2005; Zhu et al., 1997; Zhu et al., 1998). END-1 and END-3 then trigger the expression of the differentiation GATA factors ELT-7 and ELT-2, which start to be expressed at the E2 and E4 stage, respectively, and persist in enterocytes until adulthood (Nair et al., 2013; Sommermann et al., 2010; Wiesenfahrt et al., 2016). ELT-2 is a major regulator of intestinal differentiation and controls the transcription of more than 80% of intestinal specific genes, including digestion enzymes, nutrient transporters and microvilli components (McGhee et al., 2009). Consequently, *elt-2* null mutants display short and irregular microvilli and die as L1 larvae but nevertheless display a continuous intestinal lumen as well as typical gut granules (Fukushige et al., 1998). This persistence of some aspects of intestinal differentiation in the absence of ELT-2 is due to the partial redundancy between ELT-2 and ELT-7 (Dineen et al., 2018; Sommermann et al., 2010). Consistently, in larvae lacking both ELT-2 and ELT-7, large portions of the intestine show neither a lumen nor gut granules (Sommermann et al., 2010).

Polarization of the intestinal epithelium and formation of the brush border are two major steps of intestinal differentiation. Polarization becomes apparent at the E16 stage when the polarity proteins PAR-3, PAR-6 and PKC-3 start to accumulate at the apical membrane of enterocytes (Achilleos et al., 2010; Leung et al., 1999; Totong et al., 2007). Some microvilli components, including the intestine

specific isoform of actin ACT-5 and the actin/membrane linker ERM-1, also start to localize at the apical membrane during the E16 stage, prior to microvilli formation (Bidaud-Meynard et al., 2021). Microvilli start to grow between the 1.5- and 2-fold stage embryonic stages, when the intestine has reached the E20 stage (Asan et al., 2016; Bidaud-Meynard et al., 2021). At this point, the apical localization of ACT-5 and ERM-1 markedly increases and additional microvilli components, in particular the actin-capping protein EPS-8, are also recruited to growing microvilli (Bidaud-Meynard et al., 2021).

Thus, polarization and the first apical accumulation of brush border components occur at the E16 stage while microvilli formation starts at the E20 stage once the cell cycle is arrested in all intestinal cells. Here we first ask whether the timing of those differentiation steps is linked to the timing of cell divisions. By using a *cdc-25(gof)* mutation that accelerates intestinal division, we show that there is no precocious polarization or brush border formation when intestinal cells divide faster, indicating that differentiation is not triggered by the number of divisions undergone by intestinal cells. We next tested the effect of delaying cell cycle arrest by inducing the degradation of the cell cycle inhibitor CKI-1. We found that only some aspects of brush border formation are delayed when intestinal cells undergo an extra-round of divisions, thereby showing that some, but not all, aspects of differentiation require prior cell cycle arrest. Finally, we reciprocally assessed whether differentiation factors control intestinal divisions. Strikingly we found that the lack of ELT-2 and ELT-7 induce supernumerary intestinal divisions but that this phenomenon is restricted to the most posterior intestinal cells, suggesting that additional mechanisms, independent of the differentiation program, ensure that intestinal cells stop dividing.

Results

Acceleration of intestinal cell cycles does not lead to precocious polarization or brush border formation

In control embryos, polarization occurs at the E16 stage, just before the beginning of embryonic elongation, and brush border formation at the E20 stage, when the embryos reach the 2-fold stage (Fig.S1). We first wondered whether the timing of these intestinal differentiation steps was defined by

the number of cell cycles undergone by intestinal blastomeres. If this were the case, one would expect polarization and/or brush border formation to occur earlier in embryos in which intestinal divisions occur faster. To test this hypothesis, we took advantage of the *cdc-25.1(rr31)* gain-of-function mutation, which has been shown to accelerate intestinal cell cycles and to lead to an additional division of intestinal blastomeres (Demouchy et al., 2024; Kostić and Roy, 2002). As a consequence, *cdc-25.1(rr31)* embryos reach the E8 and E16 stage earlier than control embryos and eventually display on average 38 intestinal cells (Demouchy et al., 2024; Kostić and Roy, 2002) (Fig.S1). Consistently, we observed that control embryos reached the E16 stage prior to the beginning of embryonic elongation whereas *cdc-25.1(rr31)* embryos already had 32 intestinal cells at this same stage (Fig.1A). To assess the timing of epithelial polarization, we looked at the apical accumulation of the PAR protein PAR-3. As previously described, in control embryos, PAR-3 started to accumulate in discrete foci at the apical membrane of enterocytes at the early E16 stage and eventually formed a continuous apical line later during the E16 stage, when the embryo was about to start elongating (Fig.1A) (Achilleos et al., 2010). In *cdc-25.1(rr31)* embryos, foci started to accumulate at the early E32 stage and formed a continuous line later during the E32 stage, short prior to the beginning of elongation (Fig.1A). By contrast, no apical PAR-3 foci were observed at the E16 stage (Fig.1A). Thus, although intestinal cells divide faster in *cdc-25.1(rr31)* embryos, they do not polarize prematurely, indicating that reaching the E16 stage is not sufficient to trigger polarization. We next examined the timing of brush border formation by analyzing the apical accumulation of the brush border proteins ERM-1 and EPS-8. In control embryos, ERM-1 and EPS-8 progressively accumulated at the apical membrane during the first steps of embryonic elongation, as microvilli start to grow (Fig.1B-C) (Bidaud-Meynard et al., 2021). No precocious accumulation of either ERM-1 (Fig.1B) or EPS-8 (Fig1.C) was observed in *cdc-25.1(rr31)* embryos; ERM-1 accumulation was even slightly reduced (Fig.1B). Altogether, our results thus indicate that the timing of intestinal polarization and brush border formation is not linked to the number of cell cycles undergone by intestinal blastomeres.

Retardation of cell cycle arrest delays the recruitment of some brush border components

We next asked whether cell cycle arrest was a prerequisite for brush border formation. CKI-1 was previously shown to be required for cell cycle arrest (Fig.S2A) (Kostić and Roy, 2002). We therefore used an auxin-inducible degron to specifically degrade CKI-1 in the intestine and induce the appearance of a late supplemental intestinal division (see material and methods for details). Following CKI-1 degradation, 2-fold embryos displayed around 30 intestinal cells (Fig.S2B). No increase in intestinal cell number was observed at the beginning of elongation (Fig.S2B, early lima bean stage), confirming that the supernumerary intestinal cells observed at the 2-fold stage arose from a late additional division. We first examined the effect of CKI-1 degradation on the timing of ERM-1 apical accumulation, which did not seem to be altered (Fig.2A). By contrast, we found that CKI-1 degradation delays the recruitment of EPS-8 to the apical membrane. Indeed, while EPS-8 apical accumulation became clearly apparent at the 2-fold stage in control embryos, it markedly increased only at the 3-fold stage following CKI-1 degradation (Fig.2B). This observation strongly suggests that the accumulation of EPS-8 at the apical membrane requires a prior arrest of the cell cycle, thereby pointing towards the existence of a mechanism linking the timing of at least some aspects of intestinal differentiation to cell cycle progression.

Intestinal polarization and brush border formation are not required to arrest intestinal cell divisions

We next sought to determine whether intestinal differentiation reciprocally controls cell cycle progression. We first tested whether the occurrence of two major differentiation steps, polarization and/or brush border formation, could contribute to cell cycle arrest. We first tested the possible role of polarization by degrading the polarity protein PAR-3 in intestinal cells (Fig.S3A) and found that 2-fold embryos without PAR-3 had the same number of intestinal nuclei as control embryos (Fig.S3B). We next assessed the importance of brush border formation by depleting ACT-5 (Fig.S3C), the intestinal specific form of actin, which has been shown to be required for microvilli formation (MacQueen et al., 2005) and observed that 2-fold embryos lacking ACT-5 displayed 20 intestinal nuclei

(Fig.S3D). Thus, cell cycle arrest occurs in intestinal cells independently of both polarization and brush border formation onset.

ELT-2 and ELT-7 are required to prevent the appearance of supernumerary divisions in posterior intestinal cells

We next asked whether the differentiation factors ELT-2 and ELT-7 themselves could be involved in controlling cell cycle progression. Depleting ELT-2 by RNAi was sufficient to induce strong brush border and lumen defects (Fig.S4A-B). We nevertheless found that control and *elt-2(RNAi)* 2-fold embryos both displayed 20 intestinal nuclei (Fig.3A). Similarly, *elt-7(tm840)* null mutants displayed 20 intestinal nuclei at the 2-fold stage (Fig.3B). Thus, the loss of either ELT-2 or ELT-7 is not sufficient to affect intestinal divisions. To unveil a possible redundant effect of ELT-2 and ELT-7, we next depleted ELT-2 by RNAi in *elt-7(tm840)* embryos. Interestingly, we observed the presence of supernumerary intestinal nuclei in *elt-7(tm840); elt-2(RNAi)* 2-fold embryos (Fig.3B), strongly suggesting that ELT-2 and ELT-7 act redundantly to restrict the number of intestinal cells. Importantly, we did not observe any increase in intestinal cell number in *elt-7(tm840); elt-2(RNAi)* embryos at the beginning of elongation (Fig.3B, early lima bean stage), suggesting that the presence of extra nuclei at the 2-fold stage is due to late supernumerary divisions. To test whether the presence of supernumerary intestinal nuclei was indeed due to supernumerary cell divisions and not for instance to endomitosis, we next counted the number of intestinal cells in embryos expressing both the intestinal nuclear marker *end1p*::H1::mCherry and the membrane marker *end1p*::GFP::CAAX. This showed that *elt-7(tm840); elt-2(RNAi)* 2-fold embryos do not display only supernumerary intestinal nuclei but also supernumerary intestinal cells (Fig.3C). Altogether our observations indicate that ELT-2 and ELT-7 act redundantly to prevent abnormal late divisions of intestinal cells. Notably, both the most posterior nuclei (Fig.3B) and the most posterior cells (Fig.3C) of *elt-7(tm840); elt-2(RNAi)* intestines appeared smaller than others, suggesting that extra divisions may occur in the posterior region of the intestine.

To undoubtedly determine the origin of supernumerary intestinal cells, we next recorded the late steps of intestinal development in *elt-7(tm840); elt-2(RNAi)* embryos expressing *end1p*::H1::mCherry and *end1p*::GFP::CAAX. These movies revealed that *elt-7(tm840); elt-2(RNAi)* embryos first underwent the E16 to E20 transition as described in wildtype embryos (Asan et al., 2016), with cells from both the most anterior and most posterior rings dividing once (Fig.4). However, *elt-7(tm840); elt-2(RNAi)* embryos also displayed supernumerary divisions (n=12/14 embryos) (Fig.4), which occurred on average 58 min (min/max=36/93 min, n=8) after the E20 stage and emanated from cells of the 9th intestinal ring (n=12/12 embryos with supernumerary divisions), occasionally also from the 8th intestinal ring (n=7/12 embryos with supernumerary divisions). Thus, once the intestine has reached the E20 stage, the differentiation factors ELT-2 and ELT-7 appear to be required to arrest cell divisions specifically in the most posterior enterocytes.

Posterior enterocytes undergoing a supernumerary division show an abnormally late re-accumulation of Cyclin B1

We then set out to determine whether the appearance of a late additional division in the most posterior enterocytes was associated with changes in the expression of cell cycle regulators. First, we examined the expression of cyclin B1 (CYB-1), one of the three B-type cyclins, which, together with CDK-1, ensure proper progression through M phase (van der Voet et al., 2009). In E16 stage control embryos, CYB-1::GFP was never observed in cells that had stopped dividing but accumulated in the nuclei of enterocytes from the first and last intestinal rings (rings 1 and 8) before they divided to give rise to the E20 stage intestine (n=16/16 embryos) (Fig.S5). Occasionally, nuclear accumulation of CYB-1::GFP was also visible in one or two cells of the 7th intestinal ring (n=5/16 and 2/16 embryos, respectively). These cells then also divided again, leading to the formation of an intestine composed of 21 or 22 cells. Such an occasional presence of 21 or 22 intestinal cells has been previously described (Sulston and Horvitz, 1977). Importantly, CYB-1::GFP was no longer visible once the intestine had reached the E20 (or E21/E22) cell stage (Fig.S5). Similarly, in E16 stage *elt-7(tm840)* embryos treated with control RNAi, CYB-1::GFP accumulated in the nuclei of the first and last intestinal ring enterocytes

until they divided and did not reappear in their daughter cells (n=12/12 embryos) (Fig.5A). In E16 stage *elt-7(tm840); elt-2(RNAi)* embryos, CYB-1::GFP also accumulated in the nuclei of the first and last intestinal ring enterocytes until they divided (n=11/11 embryos) (Fig.5B). CYB-1::GFP then never reappeared in the daughter cells of the first intestinal ring (n=11/11 embryos) but accumulated again in one (n=4/11 embryos) or two (n=5/11 embryos) pairs of posterior daughter cells (Fig.5B). Among these 9 embryos that displayed a late accumulation of CYB-1::GFP, 8 then underwent supernumerary late divisions. In 2/11 embryos, CYB-1::GFP did not reappear in the posterior daughter cells; no supernumerary division was observed in those embryos. Thus, in the absence of ELT-2 and ELT-7, the abnormally late expression of the mitotic cyclin CYB-1 precedes the supernumerary division of the most posterior intestinal cells.

CKI-1 accumulation is delayed in posterior enterocytes undergoing a supernumerary division

We then examined whether the loss of ELT-2 and ELT-7 alters the expression of the cell cycle inhibitor CKI-1. During the E16/E20 transition in control embryos, GFP::CKI-1 transiently accumulated in the nuclei of the cells produced by the division of the first and last intestinal rings (Fig.S6A-B). A weak nuclear signal sometimes preceded division: this signal was visible in n=6/10 and 4/10 embryos for anterior and posterior cells, respectively, and appeared on average 20 min before division. GFP::CKI-1 then accumulated in the nuclei of anterior and posterior daughter cells just after division: 7/10 embryos displayed an accumulation in anterior nuclei (6 in both pairs of daughter cells, 1 in only one pair) and 9/10 in posterior nuclei (7 in both pairs of daughter cells and 2 in only one pair). GFP::CKI-1 levels then progressively decreased until no more GFP::CKI-1 could be detected (on average 35 and 40 minutes after the division of anterior and posterior cells, respectively) (Fig.S6A-B). GFP::CKI-1 displayed a similar transient accumulation in E16/E20 stage *elt-7(tm840)* embryos treated with control RNAi (Fig.6A-B): prior to the division of anterior and posterior cells, a weak nuclear signal was visible in n=8/10 and 4/10 embryos, respectively; after division, GFP::CKI-1 accumulated in the nuclei of anterior and posterior daughter cells (in all anterior daughter cell nuclei in n=10/10 embryos, in all posterior daughter cell nuclei in 9/10 embryos and in one pair of posterior daughter cells in 1/10 embryo). In

E16/E20 stage *elt-7(tm840); elt-2(RNAi)* embryos, GFP::CKI-1 also transiently accumulated in the two most anterior intestinal nuclei: it was visible in 2/9 embryos before division and in 8/9 embryos after division (in all anterior daughter cells in 6/9 embryos and in one pair of anterior daughter cells in 2/9 embryos) (Fig.6C). By contrast, when the two most posterior intestinal cells divided, GFP::CKI-1 was detected in 1/9 embryo prior to division and in none or only one pair of daughter cells after division in 5/9 and 4/9 embryos, respectively (Fig.6D). Among these 9 embryos, at least 8 then underwent late supernumerary divisions, with 7/8 showing a late nuclear accumulation of GFP::CKI-1 in supernumerary cells (Fig.6D). Our observations thus show that, during the E16/E20 transition, CKI-1 normally transiently accumulates in the nuclei of anterior and posterior intestinal cells once they have undergone their last division. This accumulation is likely to drive cell cycle arrest. However, in the absence of ELT-2 and ELT-7, the accumulation of CKI-1 in posterior nuclei after the E16/E20 division is severely reduced; this lack of CKI-1 accumulation probably contributes to the ability of posterior cells to divide one more time.

Altogether, our results demonstrate that ELT-2 and ELT-7 are required to prevent to occurrence of supernumerary late divisions in posterior intestinal cells. In the absence of ELT-2 and ELT-7, posterior intestinal cells do not accumulate the cell cycle inhibitor CKI-1 after the E16/E20 transition but rather re-accumulate cyclin B1, a major regulator of the G2/M transition. Those changes in the accumulation of cell cycle regulators are likely to drive the appearance of a supernumerary division.

Discussion

In this study, we addressed how cell proliferation and differentiation are regulated during development by using the *C. elegans* intestine as a model system. We have shown that acceleration of intestinal divisions does not impact the timing of differentiation whereas delaying cell cycle arrest postpone the recruitment of some brush border components. Reciprocally, we also have found that

differentiation factors are required to restrain intestinal divisions, although this function surprisingly appears to be restricted to the most posterior intestinal cells.

The first signs of intestinal differentiation, namely polarization and apical recruitment of some microvilli components such as ERM-1, are visible at the E16, when most intestinal have ceased dividing and during the long interphase that precedes the last division of the most anterior and posterior intestinal cells (Achilleos et al., 2010; Bidaud-Meynard et al., 2021; Leung et al., 1999; Totong et al., 2007). The next important steps of differentiation, including gut granules formation, microvilli growth and nutrient transporter expression, are initiated at the lima bean, 2-fold and 3-fold stage, respectively, once the intestine has reached the E20 stage and all intestinal cells have undergone cell cycle arrest (Asan et al., 2016; Bidaud-Meynard et al., 2019; Hermann et al., 2005 and our unpublished observations). This led us to wonder whether the timing of intestinal cell divisions and differentiation were regulated by two independent timers that happen to coincide or whether some mechanisms exist to actively coordinate the two processes. In the latter case, we hypothesized that either the number of cell divisions undergone by intestinal cells could be used as a clock controlling differentiation or that the cell cycle status, namely cell cycle arrest, could be the trigger for differentiation. We find that acceleration of the cell cycle induced by a *cdc-25.1* gain-of-function mutation leads neither to the premature polarization of intestinal nor to the precocious recruitment of brush border components. Thus, the number of divisions undergone by intestinal cells is not sufficient to provide the temporal information required to induce differentiation in a timely manner. By contrast, we show that degrading the cell cycle inhibitor CKI-1 in intestinal cells in order to delay cell cycle arrest is sufficient to delay the apical recruitment of the brush border component EPS-8. These observations indicate that CKI-1 is required to induce the timely recruitment of some brush border components, thereby revealing its ability to couple cell cycle arrest with some aspects of intestinal differentiation.

The mechanisms by which CKI-1 degradation delays EPS-8 recruitment remain to be investigated. This effect could be due to the delay in cell cycle arrest per se and to the prolonged activity of cyclin-CDK

complexes. Notably, cyclin-CDK complexes have been shown to regulate actin-binding proteins, for instance both cyclin B1-CDK1 and cyclin D1-CDK4/6 phosphorylate filamin (Cukier et al., 2007; Zhong et al., 2010), an actin cross-linker whose homolog FLN-2 accumulates at the base of microvilli in *C. elegans* (Bidaud-Meynard et al., 2019). Moreover, in *C. elegans* enterocytes, enterohemorrhagic *E. coli* intriguingly induce microvilli effacement and redistribution of ACT-5 to the cytoplasm in a CDK-1 dependent manner. This effect of CDK-1 on ACT-5 involves the phosphorylation of the formin CYK-1 by CDK-1 (Huang et al., 2021). It is therefore plausible that introducing an additional cell cycle modifies actin dynamics and impairs the recruitment of brush border components through the abnormally late activity of cyclin-CDK complexes. Alternatively, it is possible that the delayed recruitment of EPS-8 is not directly due to prolonged cell cycle but to the lack of a cell-cycle independent function CKI-1. CKI homologues have for instance been shown to promote muscle and neuronal differentiation by stabilizing the MyoD and Neurogenin 2 transcription factors, respectively (Nguyen et al., 2006; Reynaud et al., 2000; Vernon and Philpott, 2003; Vernon et al., 2003). They are also able to regulate the cytoskeleton through the Rho/ROCK/LIMK/cofilin pathway (Besson et al., 2008). In the *C. elegans* intestine, the loss of CKI-1 does not seem to delay all aspects of intestinal differentiation. In particular, ERM-1 apical recruitment appears to be unaffected, suggesting that CKI-1 is unlikely to control brush border formation through the regulation of the differentiation factors ELT-2 and ELT-7. It is however possible that the loss of CKI-1 induces alterations in the Rho/ROCK/LIMK/cofilin pathway, thereby modifying the dynamics of actin filaments and the recruitment of actin-binding proteins such as EPS-8.

Our results indicate that the timing of some aspects of brush border formation is regulated by the cell cycle status and/or CKI-1. It is however noteworthy that delaying cell cycle arrest does not seem to hamper the apical recruitment of ERM-1. This strongly suggests that early aspects of differentiation, such as ERM-1 apical recruitment, which normally occur at the E16 stage, that is before the last intestinal divisions, are not temporally regulated by cell cycle arrest; by contrast, later steps of differentiation, including EPS-8 apical recruitment, which normally occur at the E20 stage when all

intestinal cells have ceased dividing, may rely on cell cycle regulators. These observations confirm that the relationships between cell cycle and differentiation are dependent on the developmental context. The ability of cells to at least initiate differentiation before cell cycle arrest may favor a smooth transition from undifferentiated progenitors to fully differentiated post-mitotic cells and help to produce of a sufficient pool of differentiated cells in tissues with a high demand for cell production such as the epidermis (Cockburn et al., 2022). By contrast, the dependence of late differentiation steps on cell cycle arrest may ensure that highly specialized structures such as the brush border do not form in cells that will divide again.

While our first results indicated that cell cycle regulators control some aspects of intestinal differentiation, we next asked whether differentiation factors reciprocally regulate the ability of intestinal cells to divide. Previous studies have shown that the properties of intestinal cell cycles are tightly linked to the acquisition of intestinal cell fate. Intestinal specification is in particular both necessary and sufficient to control the number of intestinal cell divisions. Pioneering work has indeed shown that isolated E blastomeres divide to produce a 16-20 cell cyst-like structure, indicating that they contain most of the information required to control the number of intestinal cell cycles (Leung et al., 1999). It was also shown that defects in intestinal specification lead to the appearance of supernumerary E descendants, suggesting that specification signals restrict the number of intestinal divisions (Choi et al., 2017; Robertson et al., 2014). It is however noteworthy that several hours separate intestinal specification and cell cycle arrest, raising the question of the signal that may act as a relay between specification factors and exit of the cell cycle. Our observations demonstrate that, although specific differentiation steps, namely polarization and brush border formation, do not trigger cell cycle arrest, the differentiation factors ELT-2 and ELT-7 themselves prevent the occurrence of some late intestinal divisions. Our results show that ELT-2 and ELT-7 allow the accumulation of CKI-1 in posterior intestinal cells after the E16/E20 transition. In the absence of ELT-2 and ELT-7, the lack of CKI-1 accumulation in posterior cells after the E16 to E20 division is likely to contribute to their ability to reenter the cell cycle, to re-accumulate cyclin B1 and divide once more.

In mammals several GATA factors have been shown to directly promote the transcription of CKI homologues (Agnihotri et al., 2009; Papetti et al., 2010; Xu et al., 2021), suggesting that ELT-2 and ELT-7 could directly control CKI-1 expression. Nevertheless, although ELT-2 and ELT-7 start to be expressed in all intestinal cells from the E2/E4 stages on (Nair et al., 2013; Sommermann et al., 2010), our results strikingly show that they do not inhibit divisions prior to the E20 stage but rather specifically prevent the late occurrence of supernumerary divisions in the most posterior intestinal cells. These observations suggest that additional mechanisms ensure cell cycle progression during early intestinal development and that posterior cells are more prone to escape cell cycle arrest once the intestine has reached the E20 stage. Posterior intestinal cells distinguish themselves from more anterior cells in particular by the expression of two Hox transcription factors, NOB-1 and PHP-3 (Liu and Murray, 2023; Murray et al., 2022; Zhao et al., 2010). Interestingly, Hox family members have been shown to promote proliferation in *C. elegans* (Heinze et al., 2023; Roiz et al., 2016), raising the possibility that the presence of NOB-1 and/or PHP-3 in posterior cells could contribute to their ability to undergo supernumerary divisions in the absence of ELT-2 and ELT-7.

In conclusion, our work reveals the existence of reciprocal interactions between the cell proliferation and cell differentiation programs during the development of the C*. elegans* intestine. We show on one hand that delaying cell cycle arrest hampers the recruitment of some brush border components. On the other hand, we find that the differentiation factors ELT-2 and ELT-7 are required to prevent late supernumerary divisions in posterior intestinal cells. These mechanisms are likely to be important to coordinate intestinal differentiation with intestinal divisions. We however find that not all differentiation steps require prior cell cycle arrest and, reciprocally, that cell cycle arrest in most intestinal cells does not rely on differentiation factors. This study thus underlines that proliferation and differentiation are only partially coupled, suggesting the existence of additional mechanisms ensuring their temporal control.

Materials and Methods

Worm strains

Strains were grown on agar plates containing NGM growth media and seeded with *E. coli* (OP50 strain) and maintained at 20°C. The strains used in this study are listed in Table S1.

New CRISPR strains

CRISPR-CAS9-genome edited CKI-1::AID::BFP strain was generated at the SEGiCel facility (SFR Santé Lyon Est, CNRS UAR 3453, Lyon, France). It was obtained by inserting a GASGASGAS linker, an Auxin Inducible Degron (AID, MPKDPAKPPAKAQVVGWPPVRSYRKNVMVSCQKSSGGPEAAAFVK) (Zhang et al., 2015), a GGGGSGGGG linker and tagBFP2 to the C-terminus of CKI-1.

Auxin induced degradation

Intestine specific degradation of CKI-1 was induced by incubating at 20°C embryos expressing CKI-1::AID::BFP and the auxin receptor TIR-1 under the control of the *elt-2* promoter in 5 mM IAA-AM (acetoxymethyl indole-3-acetic acid, a cell permeable form of auxin which is able to trigger degradation in embryos (Negishi et al., 2019)). After 4 h of auxin treatment, all 2-fold embryos displayed supernumerary enterocytes, suggesting that CKI-1 was efficiently degraded. The effect of extra intestinal cell divisions on ERM-1 and EPS-8 apical accumulation was measured in comma to 3-fold embryos after 4 h of auxin treatment.

RNAi vectors and feeding conditions

RNAi was performed by feeding worms with RNAi clones 48 h on 1 mM IPTG plates. L4440 was used as a control (Timmons and Fire, 1998). For *elt-2* RNAi, a 555bp fragment amplified from the *elt-2* genomic sequence (oligos F-tacaacaaatcaatacagg and R-ataaaagttgatcacgtacc) was cloned into a Gateway compatible L4440 vector.

Microscopy and time-lapse recordings

For still imaging of live embryos, embryos were mounted on 2% agarose pads in a drop of M9 medium enriched in OP50 bacteria to immobilize embryos. Standard confocal images were acquired with a SP8 confocal microscope (Leica) equipped with a HC Plan-Apo 63×, 1.4 NA objective and the LAS AF

software. Z-stacks were acquired with 300 or 400 nm steps. Superresolution images were acquired with a LSM 880 microscope (Zeiss), equipped with a Plan-Apo 63×, 1.4 NA objective and the Zen Black software. The Airy Scan module was used to obtain superresolution images.

For time-lapse experiments, adult hermaphrodites were dissected in M9 medium. Embryos were then transferred to a 4 µL drop of M9 medium on a 35 mm glass bottom dish (poly-D-lysine coated, 14 mm microwell, No 1.5 coverglass, MatTek). Excess of M9 was then removed to ensure adhesion of embryos to poly-D-Lysine and 2 mL of mineral oil (Light Oil (neat), Sigma) was used to cover the drop of M9. Recordings were performed on a Leica DMi8 spinning disc microscope equipped with a HCX Plan-Apo 63×, 1.4 NA objective and a photometrics Evolve EMCCD camera. The setup was controlled by the Inscoper Imaging Suite. Embryos were maintained at 23°C during recordings. Images were acquired at 3 minutes intervals. Z-stacks were acquired with 400 nm steps.

Image analysis and quantifications

Images were assembled for illustration using the Fiji and Inkscape 1.1 softwares. All embryos are oriented with the anterior pole to the left. Max intensity z-projections were obtained with Fiji. Quantifications of ERM-1 and EPS-8 apical levels were performed with Fiji, by measuring mean fluorescence intensity along a segmented line covering the whole intestine (E16 to 2-fold embryos) or the visible part of the anterior intestine (3-fold embryos). Fig.3A-B, Fig.S2B, Fig.S3B,D and Fig.S4A have been post-treated with a 3D Gaussian filter(X sigma=2, Y sigma=2, Z sigma=2, Fiji). Fig.S3C has been post-treated with a 3D Gaussian filter (X sigma=1, Y sigma=1, Z sigma=1, Fiji). All the movies have been post-treated with a 3D Gaussian filter (X sigma=2, Y sigma=2, Z sigma=2, Fiji).

Statistical analysis

Statistical analysis and graphic representations were performed with the Graphpad Prism 10.0.3 software. Graphs show all individual values (dots), the median and the standard deviation (black lines). Details of the statistical tests used are indicated in each figure legend. Two-tailed unpaired Student's t tests were performed when data passed the Shapiro and Kolmogorov-Smirnov normality tests and

when sample variance was equal; two-tailed Welch's t tests were performed when data passed the Shapiro and Kolmogorov-Smirnov normality tests and when sample variance was unequal; two-tailed non-parametric Mann-Whitney tests were performed when data did not pass the Shapiro or Kolmogorov-Smirnov normality test.

Acknowledgments

We thank M. Boxem, J. Sepers and H. Pires for kindly sharing their GFP::degron::PAR-3 strain prior to publication as well as V. Gobel, K. Kemphues, M. Maduro, M. Soto and the *Caenorhabditis* Genetics Center (funded by the National Institute of Health Office of Research Infrastructure Programs, P40 OD010440) for providing worm strains. The CKI-1::degron strain was generated by the SEGiCel Facility (SFR Santé Lyon Est, CNRS UAR 3453, Lyon, France). M. Kanemaki provided us with modified auxin. We thank the Michaux and Pecreaux labs as well as L. Pintard, F. Pituello and L. Bataillé for valuable discussions. Imaging was performed at the Microscopy Rennes imaging Center (MRiC Photonics, Biosit, Rennes, France), a member of the national infrastructure France-BioImaging supported by the French National Research Agency (ANR-10-INBS-04).

Funding

This work was supported by the Ligue Contre le Cancer (22, 35), the Fondation ARC (PJA 20191209366), the Fondation Maladies Rares (EXM-2019-1013) and the ANR (GroBluRe). GM laboratory also received institutional funding from the Centre National de la Recherche Scientifique and the Université de Rennes. The authors declare no competing financial interests.

Author contributions

Conceptualization: J.D., G.M., A.P.; Methodology: J.D., A.P.; Validation: J.D., G.M., A.P.; Formal analysis: J.D., A.P.; Investigation: J.D.; Writing – original draft preparation: J.D., A.P.; Writing – Review and editing: J.D., G.M., A.P.; Vizualization: J.D.; Supervision: G.M., A.P.; Project administration: G.M.; Funding Acquisition: G.M., A.P.

References

Achilleos, A., Wehman, A. M. and Nance, J. (2010). PAR-3 mediates the initial clustering and apical localization of junction and polarity proteins during C. elegans intestinal epithelial cell polarization. *Development* **137**, 1833–1842.

Adikes, R. C., Kohrman, A. Q., Martinez, M. A. Q., Palmisano, N. J., Smith, J. J., Medwig-Kinney, T. N., Min, M., Sallee, M. D., Ahmed, O. B., Kim, N., et al. (2020). Visualizing the metazoan proliferation-quiescence decision in vivo. *eLife* **9**, e63265.

Agnihotri, S., Wolf, A., Picard, D., Hawkins, C. and Guha, A. (2009). GATA4 is a regulator of astrocyte cell proliferation and apoptosis in the human and murine central nervous system. *Oncogene* **28**, 3033–3046.

Asan, A., Raiders, S. A. and Priess, J. R. (2016). Morphogenesis of the C. elegans Intestine Involves Axon Guidance Genes. *PLoS Genet* **12**, e1005950.

Bao, Z., Zhao, Z., Boyle, T. J., Murray, J. I. and Waterston, R. H. (2008). Control of cell cycle timing during C. elegans embryogenesis. *Dev Biol* **318**, 65–72.

Besson, A., Dowdy, S. F. and Roberts, J. M. (2008). CDK inhibitors: cell cycle regulators and beyond. *Dev Cell* **14**, 159–169.

Bidaud-Meynard, A., Nicolle, O., Heck, M., Le Cunff, Y. and Michaux, G. (2019). A V0-ATPase-dependent apical trafficking pathway maintains the polarity of the intestinal absorptive membrane. *Development* **146**, dev174508.

Bidaud-Meynard, A., Demouchy, F., Nicolle, O., Pacquelet, A., Suman, S. K., Plancke, C. N., Robin, F. B. and Michaux, G. (2021). High-resolution dynamic mapping of the C. elegans intestinal brush border. *Development* **148**, dev200029.

Boxem, M. and Van Den Heuvel, S. (2001). *lin-35* Rb and *cki-1* Cip/Kip cooperate in developmental regulation of G1 progression in *C. elegans*. *Development* **128**, 4349–4359.

Castiglioni, V. G., Pires, H. R., Rosas Bertolini, R., Riga, A., Kerver, J. and Boxem, M. (2020). Epidermal PAR-6 and PKC-3 are essential for larval development of C. elegans and organize non-centrosomal microtubules. *Elife* **9**,.

Choi, H., Broitman-Maduro, G. and Maduro, M. F. (2017). Partially compromised specification causes stochastic effects on gut development in C. elegans. *Dev Biol* **427**, 49–60.

Clucas, C., Cabello, J., Büssing, I., Schnabel, R. and Johnstone, I. L. (2002). Oncogenic potential of a C.elegans cdc25 gene is demonstrated by a gain-of-function allele. *EMBO J* **21**, 665–674.

Cockburn, K., Annusver, K., Gonzalez, D. G., Ganesan, S., May, D. P., Mesa, K. R., Kawaguchi, K., Kasper, M. and Greco, V. (2022). Gradual differentiation uncoupled from cell cycle exit generates heterogeneity in the epidermal stem cell layer. *Nat Cell Biol* **24**, 1692–1700.

Cukier, I. H., Li, Y. and Lee, J. M. (2007). Cyclin B1/Cdk1 binds and phosphorylates Filamin A and regulates its ability to cross-link actin. *FEBS Lett* **581**, 1661–1672.

Demouchy, F., Nicolle, O., Michaux, G. and Pacquelet, A. (2024). PAR-4/LKB1 prevents intestinal hyperplasia by restricting endoderm specification in Caenorhabditis elegans embryos. *Development* **151**, dev202205.

Dineen, A., Osborne Nishimura, E., Goszczynski, B., Rothman, J. H. and McGhee, J. D. (2018). Quantitating transcription factor redundancy: The relative roles of the ELT-2 and ELT-7 GATA factors in the C. elegans endoderm. *Dev Biol* **435**, 150–161.

Edgar, L. G. and McGhee, J. D. (1988). DNA synthesis and the control of embryonic gene expression in C. elegans. *Cell* **53**, 589–599.

Fukushige, T., Hawkins, M. G. and McGhee, J. D. (1998). The GATA-factor elt-2 is essential for formation of the Caenorhabditis elegans intestine. *Developmental Biology* **198**, 286–302.

Heinze, S. D., Berger, S., Engleitner, S., Daube, M. and Hajnal, A. (2023). Prolonging somatic cell proliferation through constitutive hox gene expression in C. elegans. *Nat Commun* **14**, 6850.

Hermann, G. J., Schroeder, L. K., Hieb, C. A., Kershner, A. M., Rabbitts, B. M., Fonarev, P., Grant, B. D. and Priess, J. R. (2005). Genetic analysis of lysosomal trafficking in Caenorhabditis elegans. *Mol Biol Cell* **16**, 3273–3288.

Huang, C.-R., Kuo, C.-J., Huang, C.-W., Chen, Y.-T., Liu, B.-Y., Lee, C.-T., Chen, P.-L., Chang, W.-T., Chen, Y.-W., Lee, T.-M., et al. (2021). Host CDK-1 and formin mediate microvillar effacement induced by enterohemorrhagic Escherichia coli. *Nat Commun* **12**, 90.

Kostić, I. and Roy, R. (2002). Organ-specific cell division abnormalities caused by mutation in a general cell cycle regulator in C. elegans. *Development* **129**, 2155–2165.

Lee, Y.-U., Son, M., Kim, J., Shim, Y.-H. and Kawasaki, I. (2016). CDC-25.2, a C. elegans ortholog of cdc25, is essential for the progression of intestinal divisions. *Cell Cycle* **15**, 654–666.

Leung, B., Hermann, G. J. and Priess, J. R. (1999). Organogenesis of the Caenorhabditis elegans intestine. *Dev. Biol.* **216**, 114–134.

Liu, J. and Murray, J. I. (2023). Mechanisms of lineage specification in Caenorhabditis elegans. *Genetics* **225**, iyad174.

Lobjois, V., Bel-Vialar, S., Trousse, F. and Pituello, F. (2008). Forcing neural progenitor cells to cycle is insufficient to alter cell-fate decision and timing of neuronal differentiation in the spinal cord. *Neural Dev* **3**, 4.

MacQueen, A. J., Baggett, J. J., Perumov, N., Bauer, R. A., Januszewski, T., Schriefer, L. and Waddle, J. A. (2005). ACT-5 is an essential Caenorhabditis elegans actin required for intestinal microvilli formation. *Mol. Biol. Cell* **16**, 3247–3259.

Maduro, M. F., Hill, R. J., Heid, P. J., Newman-Smith, E. D., Zhu, J., Priess, J. R. and Rothman, J. H. (2005). Genetic redundancy in endoderm specification within the genus Caenorhabditis. *Developmental Biology* **284**, 509–522.

Martinez, M. A. Q., Zhao, C. Z., Moore, F. E. Q., Yee, C., Zhang, W., Shen, K., Martin, B. L. and Matus, D. Q. (2024). Cell cycle perturbation uncouples mitotic progression and invasive behavior in a post-mitotic cell. *Differentiation* **137**, 100765.

McGhee, J. D., Sleumer, M. C., Bilenky, M., Wong, K., McKay, S. J., Goszczynski, B., Tian, H., Krich, N. D., Khattra, J., Holt, R. A., et al. (2007). The ELT-2 GATA-factor and the global regulation of transcription in the C. elegans intestine. *Dev Biol* **302**, 627–645.

McGhee, J. D., Fukushige, T., Krause, M. W., Minnema, S. E., Goszczynski, B., Gaudet, J., Kohara, Y., Bossinger, O., Zhao, Y., Khattra, J., et al. (2009). ELT-2 is the predominant transcription factor

controlling differentiation and function of the C. elegans intestine, from embryo to adult. *Developmental Biology* **327**, 551–565.

Murray, J. I., Preston, E., Crawford, J. P., Rumley, J. D., Amom, P., Anderson, B. D., Sivaramakrishnan, P., Patel, S. D., Bennett, B. A., Lavon, T. D., et al. (2022). The anterior Hox gene ceh-13 and elt-1/GATA activate the posterior Hox genes nob-1 and php-3 to specify posterior lineages in the C. elegans embryo. *PLoS Genet* **18**, e1010187.

Nair, G., Walton, T., Murray, J. I. and Raj, A. (2013). Gene transcription is coordinated with, but not dependent on, cell divisions during C. elegans embryonic fate specification. *Development* **140**, 3385–3394.

Negishi, T; Asakawa, M; Kanemaki, MT; Sawa, H (2019). Modified auxin improves the auxin-inducible degradation (AID) system for laid C. elegans embryos.

Nguyen, L., Besson, A., Heng, J. I.-T., Schuurmans, C., Teboul, L., Parras, C., Philpott, A., Roberts, J. M. and Guillemot, F. (2006). p27kip1 independently promotes neuronal differentiation and migration in the cerebral cortex. *Genes Dev* **20**, 1511–1524.

Papetti, M., Wontakal, S. N., Stopka, T. and Skoultchi, A. I. (2010). GATA-1 directly regulates p21 gene expression during erythroid differentiation. *Cell Cycle* **9**, 1972–1980.

Reynaud, E. G., Leibovitch, M. P., Tintignac, L. A., Pelpel, K., Guillier, M. and Leibovitch, S. A. (2000). Stabilization of MyoD by direct binding to p57(Kip2). *J Biol Chem* **275**, 18767–18776.

Robertson, S. M., Medina, J. and Lin, R. (2014). Uncoupling different characteristics of the C. elegans E lineage from differentiation of intestinal markers. *PLoS One* **9**, e106309.

Roiz, D., Escobar-Restrepo, J. M., Leu, P. and Hajnal, A. (2016). The C. elegans hox gene lin-39 controls cell cycle progression during vulval development. *Dev Biol* **418**, 124–134.

Ruijtenberg, S. and van den Heuvel, S. (2016). Coordinating cell proliferation and differentiation: Antagonism between cell cycle regulators and cell type-specific gene expression. *Cell Cycle* **15**, 196–212.

Sasidharan, S., Borinskaya, S., Patel, F., Bernadskaya, Y., Mandalapu, S., Agapito, M. and Soto, M. C. (2018). WAVE regulates Cadherin junction assembly and turnover during epithelial polarization. *Dev Biol* **434**, 133–148.

Sommermann, E. M., Strohmaier, K. R., Maduro, M. F. and Rothman, J. H. (2010). Endoderm development in Caenorhabditis elegans: the synergistic action of ELT-2 and -7 mediates the specification→differentiation transition. *Dev. Biol.* **347**, 154–166.

Spike, C. A., Tsukamoto, T. and Greenstein, D. (2022). Ubiquitin ligases and a processive proteasome facilitate protein clearance during the oocyte-to-embryo transition in Caenorhabditis elegans. *Genetics* **221**, iyac051.

Sulston, J. E. and Horvitz, H. R. (1977). Post-embryonic cell lineages of the nematode, Caenorhabditis elegans. *Dev Biol* **56**, 110–156.

Sulston, J. E., Schierenberg, E., White, J. G. and Thomson, J. N. (1983). The embryonic cell lineage of the nematode Caenorhabditis elegans. *Developmental Biology* **100**, 64–119.

Timmons, L. and Fire, A. (1998). Specific interference by ingested dsRNA. *Nature* **395**, 854.

Totong, R., Achilleos, A. and Nance, J. (2007). PAR-6 is required for junction formation but not apicobasal polarization in C. elegans embryonic epithelial cells. *Development* **134**, 1259–1268.

van der Voet, M., Lorson, M. A., Srinivasan, D. G., Bennett, K. L. and van den Heuvel, S. (2009). C. elegans mitotic cyclins have distinct as well as overlapping functions in chromosome segregation. *Cell Cycle* **8**, 4091–4102.

Vernon, A. E. and Philpott, A. (2003). A single cdk inhibitor, p27Xic1, functions beyond cell cycle regulation to promote muscle differentiation in Xenopus. *Development* **130**, 71–83.

Vernon, A. E., Devine, C. and Philpott, A. (2003). The cdk inhibitor p27Xic1 is required for differentiation of primary neurones in Xenopus. *Development* **130**, 85–92.

Wehman, A. M., Poggioli, C., Schweinsberg, P., Grant, B. D. and Nance, J. (2011). The P4-ATPase TAT-5 inhibits the budding of extracellular vesicles in C. elegans embryos. *Curr Biol* **21**, 1951–1959.

Wiesenfahrt, T., Berg, J. Y., Osborne Nishimura, E., Robinson, A. G., Goszczynski, B., Lieb, J. D. and McGhee, J. D. (2016). The function and regulation of the GATA factor ELT-2 in the C. elegans endoderm. *Development* **143**, 483–491.

Willms, R. J., Zeng, J. and Campbell, S. D. (2020). Myt1 Kinase Couples Mitotic Cell Cycle Exit with Differentiation in Drosophila. *Cell Rep* **33**, 108400.

Wong, M.-K., Ho, V. W. S., Huang, X., Chan, L.-Y., Xie, D., Li, R., Ren, X., Guan, G., Ma, Y., Hu, B., et al. (2022). Initial characterization of gap phase introduction in every cell cycle of C. elegans embryogenesis. *Front. Cell Dev. Biol.* **10**, 978962.

Xu, J., Yu, D., Dong, X., Xie, X., Xu, M., Guo, L., Huang, L., Tang, Q. and Gan, L. (2021). GATA3 maintains the quiescent state of cochlear supporting cells by regulating p27kip1. *Sci Rep* **11**, 15779.

Zhang, H., Kim, A., Abraham, N., Khan, L. A., Hall, D. H., Fleming, J. T. and Gobel, V. (2012). Clathrin and AP-1 regulate apical polarity and lumen formation during C. elegans tubulogenesis. *Development* **139**, 2071–2083.

Zhang, L., Ward, J. D., Cheng, Z. and Dernburg, A. F. (2015). The auxin-inducible degradation (AID) system enables versatile conditional protein depletion in C. elegans. *Development* **142**, 4374–4384.

Zhao, Z., Boyle, T. J., Liu, Z., Murray, J. I., Wood, W. B. and Waterston, R. H. (2010). A negative regulatory loop between microRNA and Hox gene controls posterior identities in Caenorhabditis elegans. *PLoS Genet* **6**, e1001089.

Zhong, Z., Yeow, W.-S., Zou, C., Wassell, R., Wang, C., Pestell, R. G., Quong, J. N. and Quong, A. A. (2010). Cyclin D1/cyclin-dependent kinase 4 interacts with filamin A and affects the migration and invasion potential of breast cancer cells. *Cancer Res* **70**, 2105–2114.

Zhu, J., Hill, R. J., Heid, P. J., Fukuyama, M., Sugimoto, A., Priess, J. R. and Rothman, J. H. (1997). end-1 encodes an apparent GATA factor that specifies the endoderm precursor in Caenorhabditis elegans embryos. *Genes & Development* **11**, 2883–2896.

Zhu, J., Fukushige, T., McGhee, J. D. and Rothman, J. H. (1998). Reprogramming of early embryonic blastomeres into endodermal progenitors by a Caenorhabditis elegans GATA factor. *Genes Dev* **12**, 3809–3814.

Fig.1: Acceleration of intestinal cell cycles triggered by a *cdc-25.1* gain of function mutation does not lead to precocious polarization or brush border formation. A. Maximum Z-projections from confocal images of control and *cdc-25.1(rr31) (cdc-25.1(gof))* embryos expressing PAR-3::GFP, HMR-1::mKate2 and the intestinal nuclear marker *end1p::*H1::mCherry. In *cdc-25.1(rr31)* embryos, intestinal cell divisions occur faster such that the intestine reaches the E16 stage approximately at the same time as the E8 stage in control embryos and the E32 stage before elongation initiation (also see Fig.S1). In control and *cdc-25.1(rr31)* embryos, PAR-3 apical foci (blue arrowheads) start to be visible in intestinal cells at the E16 and E32 stage, respectively. PAR-3 then forms an apical line (red arrowheads) just before the beginning of elongation. Dashed lines outline intestinal cells. **B-C.** Maximum Z-projections from confocal images of control and *cdc-25.1(rr31) (cdc-25.1(gof))* embryos expressing ERM-1::mNG (B) or EPS-8::mNG (C) at the indicated embryonic stages and quantification of ERM-1::mNG (B) and EPS-8::mNG (C) fluorescence levels in those embryos (a.u: arbitrary unit). In C, dashed lines outline the extent of the embryos; at the 3-fold stage, the fainter lines indicate the embryonic region which is folding in a lower focal plane. ns: non-significant (P>0.05), **P<0.01, Mann-Whitney test for comma stage in B and 3-fold-stage in C, Welch's t test for 1.5-fold stage in B and 2-fold stage in C, unpaired t test for 2-fold stage in B and 1.5-fold stage in C. Scale bars: 5 µm.

Fig.2: Retardation of cell cycle arrest following CKI-1 degradation induces a delay in the accumulation of the brush border component EPS-8. Maximum Z-projections from confocal images of auxin-treated embryos expressing ERM-1::mNG (A) or EPS-8::mNG (B) and either *elt-2p::*TIR-1 (Control) or both *elt-2p::*TIR-1 and CKI-1::degron::BFP (CKI-1::degron) at the indicated embryonic stages and quantification of ERM-1::mNG (A) and EPS-8::mNG (B) fluorescence levels in those embryos (a.u: arbitrary unit). In B, dashed lines outline the extent of the embryos; at the 3-fold stage, the fainter lines indicate the embryonic region which is folding in a lower focal plane. ns: non-significant (P>0.05), *P<0.05, **P<0.01, ****P<0.0001, unpaired t test for A, Welch's t test for 1.5 and 2-fold stages in B, Mann-Whitney test for 3-fold stage in C. Scale bars: 5 µm.

Fig.3: Loss of ELT-2 and ELT-7 leads to the presence of supernumerary intestinal cells. A. *(left)* Maximum Z-projections from confocal images of 2-fold embryos expressing the intestinal nuclear marker *end1p::*H1::mCherry and treated with control or *elt-2* RNAi. *(right)* quantification of the number of intestinal nuclei in those embryos. ns: non-significant (*P*>0.05, Mann-Whitney test). **B.** *(left)* Maximum Z-projections from confocal images of 2-fold *elt-7(tm840)* embryos expressing *end1p::*H1::mCherry and treated with control or *elt-2* RNAi. The *elt-7((tm840); elt-2(RNAi)* embryo shown has 25 intestinal nuclei (only 23 are visible on the maximal projection). In this embryo, the posterior nuclei (circled with dotted lines) appear smaller than other intestinal nuclei, suggesting that they may result from supernumerary intestinal divisions. *(right)* Quantification of the number of intestinal nuclei in *elt-7(tm840)* early lima bean and 2-fold embryos treated with control or *elt-2* RNAi. ns: non-significant (*P*>0.05), ****P<0.0001 (Mann-Whitney test). In A and B, dashed lines outline the extent of the embryos. **C.** *(left)* Confocal images taken at three different focal planes of *elt-7(tm840)* 2-fold embryos expressing the intestinal membrane marker *end1p*::GFP::CAAX and treated with control or *elt-2* RNAi. Dotted lines outline cells from the most anterior (white) and posterior (magenta) intestinal rings. *elt-7((tm840)* embryos have 20 intestinal cells, with 4 anterior and 4 posterior cells arising from the late intestinal divisions occurring between E16 and E20 stage. The *elt-7((tm840); elt-2(RNAi)* embryo shown has 23 intestinal cells, with 7 small posterior cells that may result from late supernumerary divisions. *(right)* Quantification of the number of intestinal cells in *elt-7(tm840)* 2-fold embryos treated with control or *elt-2* RNAi. ****P<0.0001 (Mann-Whitney test). Scale bars: 5 µm.

Fig.4: Loss of ELT-2 and ELT-7 leads to supernumerary divisions in the posterior region of the intestine. Schematic representations (upper row) and confocal images showing the first and last rings of E16 to E21 stage *elt-7(tm840)* embryos treated with *elt-2* RNAi and expressing the intestinal membrane marker *end1p*::GFP::CAAX and the intestinal nuclear marker *end1p::*H1::mCherry. White/cyan and red/yellow circles highlight the membrane of the enterocytes from the first and last intestinal ring, respectively, before (E16) and after (E17 to E20) their division. The first division of the E16 to E20 transition was used as reference for division timing (t=0). In this embryo, first ring divisions

occur between t=21 to t=27 min (cyan cells) and t=39 to t=42 min (white cells; at t=42 min 2 focal planes are shown to make the two white daughter cells visible). Last ring divisions occur at t=0 (red cells) and between t=30 to t=39 min (yellow cells). Later, between t=132 to t=135, one of the yellow daughter cells undergoes a supernumerary division. Scale bars: 5 µm

Fig.5: Loss of ELT-2 and ELT-7 is associated with the late accumulation of CYB-1::GFP in posterior enterocytes. A-B. Schematic representations (upper row) and maximum Z-projections (A) or single focal planes (B) from confocal images showing the first and last rings of E16 to E20 stage *elt-7(tm840)* embryos treated with control (A) or *elt-2* (B) RNAi and expressing the intestinal nuclear marker *end1p::*H1::mCherry and CYB-1::GFP. White/cyan and red/yellow circles highlight the nuclei of the first and last intestinal ring enterocytes, respectively, before (E16) and after (E17 to E20) their division. The first division of the E16 to E20 transition was used as reference for division timing (t=0). In the *elt-7(tm840)* embryo (A), first ring divisions occur at t=0 (white nuclei) and between t=6 to t= 24 min (cyan nuclei). Last ring divisions occur at t=6 min (yellow nuclei) and between t=6 to t= 24 min (red nuclei). CYB-1::GFP accumulates specifically in the first and last ring enterocytes prior to their division and does not reappear in their daughter cells. In the *elt-7(tm840); elt-2(RNAi)* embryo (B), first ring divisions occur at t=24 min (white nuclei) and t= 36 min (cyan nuclei). Last ring divisions occur at t=0 (red and yellow nuclei). At t=36 min, CYB-1::GFP starts to reappear in one cell of ring 9 (one of the red nuclei); at t=66 min, it is clearly visible in all cells from ring 8 and 9 (2 red and 2 yellow nuclei, 2 focal planes are shown to make the 4 nuclei visible). One of the red and one of the yellow daughter cells undergo a supernumerary division at t= 81 min and t=90 min, respectively. The other red and yellow daughter cells both undergo a supernumerary division immediately after (not shown). Scale bars: 5 µm

Fig.6: Loss of ELT-2 and ELT-7 is associated with the loss of GFP::CKI-1 accumulation in posterior enterocytes. A-D. Schematic representations (upper rows) and confocal images showing the first and last rings of E16 to E20 stage *elt-7(tm840)* embryos treated with control (A-B) or *elt-2* (C-D) RNAi and expressing the intestinal nuclear marker *end1p::*H1::mCherry and GFP::CKI-1. A single *elt-7(tm840)*

embryo and a single *elt-7(tm840)*; *elt-2(RNAi)* embryo are shown in A and B and in C and D, respectively. Focal planes were chosen to display the anterior (A and C) or posterior (B and D) cell divisions. White/cyan and yellow circles highlight the nuclei of one cell of the first and last intestinal ring enterocytes, respectively, before (E16) and after (E17 to E20) their division. The first division of the E16 to E20 transition was used as reference for division timing (t=0). In the *elt-7(tm840)* embryo, one of the first ring divisions (A) occurs at t=0 (white nuclei, only one daughter cell visible in the chosen focal plane). Division of the other anterior cell (cyan nucleus) occurs in a different focal plane and is not shown here. GFP::CKI-1 starts to be visible in the white mother cell nucleus prior to division (t=-9 min) and accumulates in the nucleus of the two white daughter cells after the division (t=6 min) and then progressively disappears until it is not any longer visible (t=66 min). One of the last ring divisions (B) occurs between t=3 and t=6 min (yellow nuclei). Division of the other posterior cell (red nucleus) occurs in a different focal plane and is not shown here. GFP::CKI-1 accumulates in the nucleus of the two yellow daughter cells after the division (t=9 min) and then progressively disappears until it is not any longer visible (t=33 min). In the *elt-7(tm840); elt-2(RNAi)* embryo, one first ring division (C) occurs at t=18 min (cyan nuclei). Division of the other anterior cell (white nucleus) occurs in a different focal plane and is not shown here. GFP::CKI-1 accumulates in the nucleus of the two cyan daughter cells after the division (t=24 min, 2 focal planes are shown to make the two daughter nuclei visible) and then progressively disappears until it is not any longer visible (t=66 min). One last ring division (D) occurs at t=0 (yellow nuclei). Division of the other posterior cell (red nucleus) occurs in a different focal plane and is not shown here. GFP::CKI-1 does not accumulate in the nucleus of the two yellow daughter cells right after the division (t=12 min). It eventually becomes visible in one of the two yellow daughters at t=81 min. This cell then undergoes a supernumerary division at t=87 min and its daughters then accumulate GFP::CKI-1 in the nucleus (t=96 min). Scale bars: 5 µm.

Fig.S1: The *cdc-25.1(rr31)* gain of function mutation leads to the acceleration of intestinal cell divisions and to the appearance of an additional division. Schematic representation of intestinal divisions in control and *cdc-25.1(rr31)* embryos. In control embryos, the E blastomeres and all its

descendants divide to successively give rise to the E2, E4, E8 and E16 stages. The most anterior and posterior cells then divide one more time to form the E20 stage. The E16 stage is reached before the start of elongation while 2-fold embryos are at the E20 stage. Polarization and brush border formation occur at the E16 and 2-fold stage, respectively. In *cdc-25.1(rr31)* embryos, intestinal cells divide faster and one more time than in control embryos, thereby containing 32 intestinal cells before elongation and about 40 intestinal cells after elongation.

Fig.S2: Loss of CKI-1 leads to the appearance of a late supplementary division of intestinal cells. **A.** Schematic representation of intestinal divisions in control embryos and in embryos lacking CKI-1. Intestinal cells divide at the same speed and both embryos have 16 intestinal cells at the beginning of elongation; in embryos lacking CKI-1, all intestinal cells then undergo an additional late division after the E16 stage so that embryos display around 32 cells during elongation (Kostić and Roy, 2002). **B.** Maximum Z-projections from confocal images of auxin-treated embryos expressing the intestinal nuclear marker *end1p::*H1::mCherry and either *elt-2p::*TIR-1 (Control) or both *elt-2p::*TIR-1 and CKI-1::degron::BFP (CKI-1::degron) at the indicated embryonic stages and quantification of intestinal nuclei number in those embryos. Asterix indicate non intestinal cells that occasionally express *end1p::*H1::mCherry. ns: non-significant (P>0.05), ****P<0.0001, Mann-Whitney test. Scale bars: 5 µm.

Fig.S3: Intestinal polarization and brush border formation are not required to arrest intestinal cell divisions. A. Maximum Z-projections from confocal images of comma embryos expressing GFP::degron::PAR-3 and *elt-2p::*TIR-1 and treated 30 min with DMSO or auxin. In the presence of auxin, PAR-3 is specifically degraded in intestinal cells. **B.** Maximum Z-projections from confocal images of auxin-treated 2-fold embryos expressing the intestinal nuclear marker *elt-2p::*NLS:: GFP and either *elt-2p::*TIR-1 (Control) or both *elt-2p::*TIR-1 and GFP::degron::PAR-3 and quantification of the number of intestinal nuclei in those embryos. ns: non-significant (P>0.05, Mann-Whitney test). **C.** Maximum Z-projections from confocal images of 2-fold embryos expressing ACT-5::GFP and treated with control

and *act-5* RNAi. ACT-5::GFP is efficiently depleted in embryos treated by *act-5* RNAi. **D** Maximum Z-projections from confocal images of 2-fold embryos expressing the intestinal specific nuclear marker ELT-2::mNG and treated with control or *act-5* RNAi and quantification of the number of intestinal nuclei in those embryos. ns: non-significant (P>0.05, Mann-Whitney test). Dashed lines outline the extent of the embryos. Scale bars: 5 µm.

Fig.S4: Loss of ELT-2 leads to strong intestinal defects. A-B. Maximum Z-projections from confocal images of 2-fold embryos expressing the intestinal nucleic marker ELT-2::mNG and treated with control or *elt-2* RNAi. Dashed lines outline the extent of the embryos **B.** Super-resolution confocal images of the intestine in 3-fold embryos expressing ERM-1::mNG and treated with control or *elt-2* RNAi. In control embryos, the intestine is characterized by a regular lumen and a well-defined brush border; on the contrary, *elt-2* RNAi treated embryos display discontinuities of the intestinal lumen (white arrowhead) and a poorly structured brush border. Scale bars: 5 µm.

Fig.S5: Expression pattern of CYB-1::GFP in control embryos. Schematic representations (upper row) and maximum Z-projections from confocal images showing the first and last rings of a E16 to E20 stage embryo expressing the intestinal nuclear marker *end1p::*H1::mCherry and CYB-1::GFP. White/cyan and red/yellow circles highlight the nuclei of the first and last intestinal ring enterocytes, respectively, before (E16) and after (E17 to E20) their division. The first division of the E16 to E20 transition was used as reference for division timing (t=0). In this embryo, the two first ring divisions occur at t=0 (white and cyan nuclei). Last ring divisions occur at t=9 min (yellow nuclei) and t= 27 min (red nuclei). CYB-1::GFP accumulates specifically in the first and last ring enterocytes prior to their division and does not reappear in their daughter cells. Scale bars: 5 µm.

Fig.S6: Expression pattern of GFP::CKI-1 in control embryos. A-B. Schematic representations (upper rows) and confocal images showing the first and last rings of a E16 to E20 stage embryo expressing the intestinal nuclear marker *end1p::*H1::mCherry and GFP::CKI-1. The same embryo is shown in A and B. Focal planes were chosen to display the anterior (A) or posterior (B) cell divisions. White and yellow

circles highlight the nuclei of one cell of the first and last intestinal ring enterocytes, respectively, before (E16) and after (E17 to E20) their division. The first division of the E16 to E20 transition was used as reference for division timing (t=0). In this embryo, one first ring division (A) occurs at t=3 min (white nucleus). Division of the other anterior cell (cyan nucleus) occurs in a different focal plane and is not shown here. GFP::CKI-1 starts to be visible in the white mother cell just prior to division (t=-3 min) and accumulates in the nucleus of the two white daughter cells after the division (t=9 min) and then progressively disappears until it is not any longer visible (t=51 min). One last ring division (B) occurs at t=0 (yellow nuclei, 2 focal planes are shown to make the two daughter nuclei visible). Division of the other posterior cell (red nucleus) occurs in a different focal plane and is not shown here. GFP::CKI-1 accumulates in the nucleus of the two yellow daughter cells just after the division (t=9min) (2 focal planes are shown to make the yellow daughter nuclei visible) and then progressively disappears until it is not any longer visible (t=57 min). Scale bars: 5 µm.

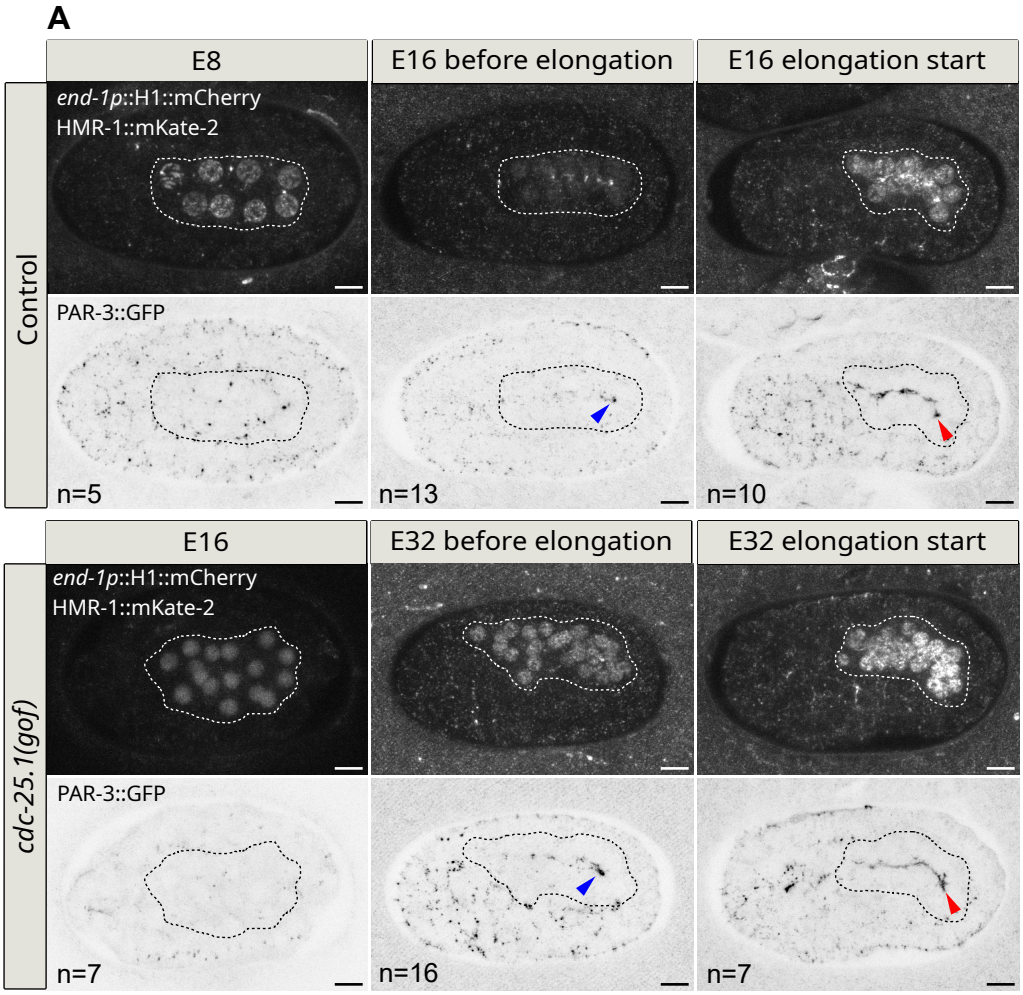
A
E8
E16 before elongation
E16 elongation start
Control
end-1p::H1::mCherry
HMR-1::mKate-2
PAR-3::GFP
n=5
n=13
n=10
E16
E32 before elongation
E32 elongation start
cdc-25.1(gof)
end-1p::H1::mCherry
HMR-1::mKate-2
PAR-3::GFP
n=7
n=16
n=7

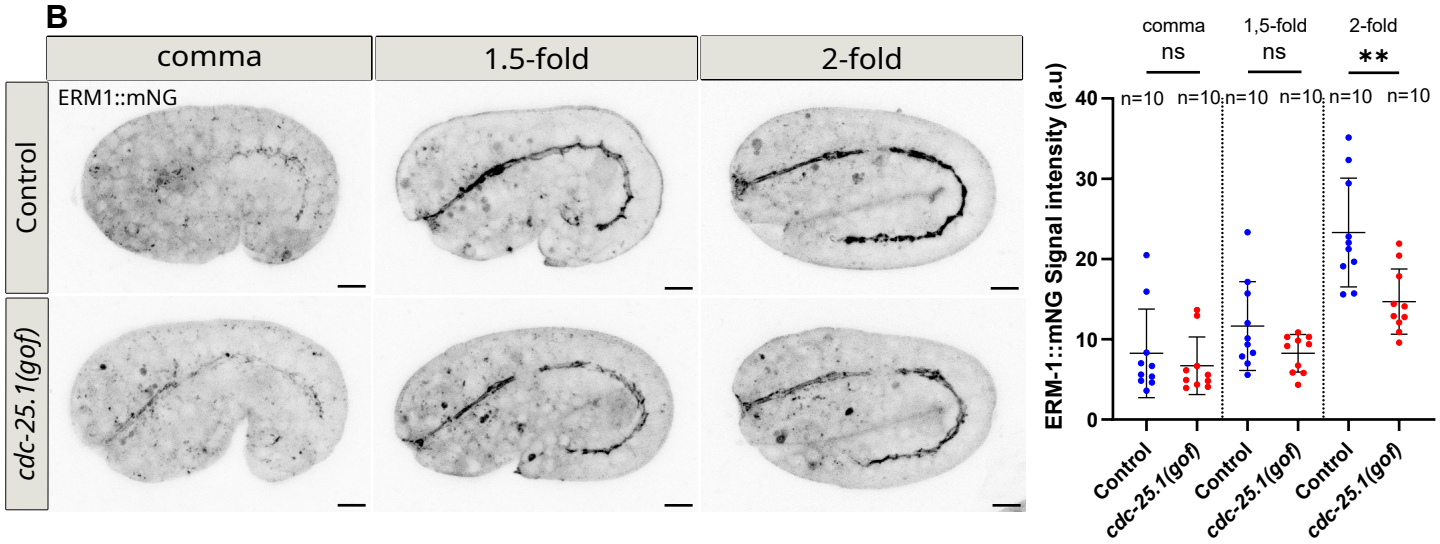
B
comma
1.5-fold
2-fold
Control
cdc-25.1(gof)
ERM1::mNG
comma
1,5-fold
2-fold
ns
ns
**
n=10 n=10 n=10 n=10 n=10 n=10
ERM-1::mNG Signal intensity (a.u)
0
10
20
30
40
Control
cdc-25.1(gof)
Control
cdc-25.1(gof)
Control
cdc-25.1(gof)

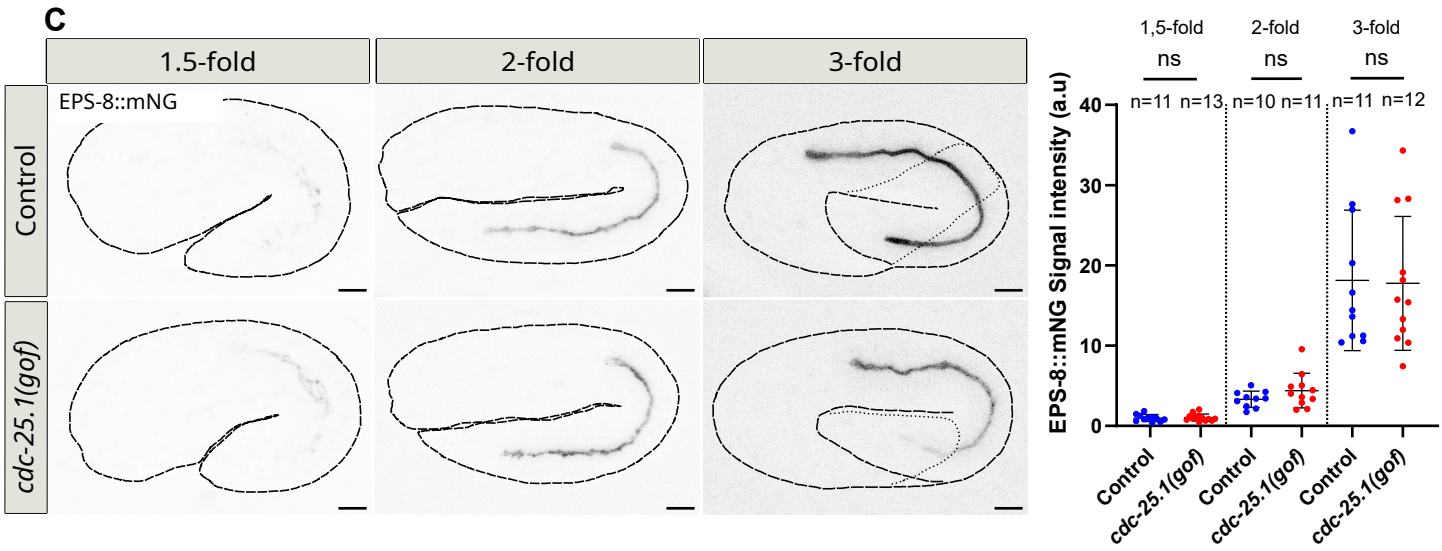
C
1.5-fold
2-fold
3-fold
Control
cdc-25.1(gof)
EPS-8::mNG
1,5-fold
2-fold
3-fold
ns
ns
ns
n=11 n=13 n=10 n=11 n=11 n=12
EPS-8::mNG Signal intensity (a.u)
0
10
20
30
40
Control
cdc-25.1(gof)
Control
cdc-25.1(gof)
Control
cdc-25.1(gof)

Figure 1

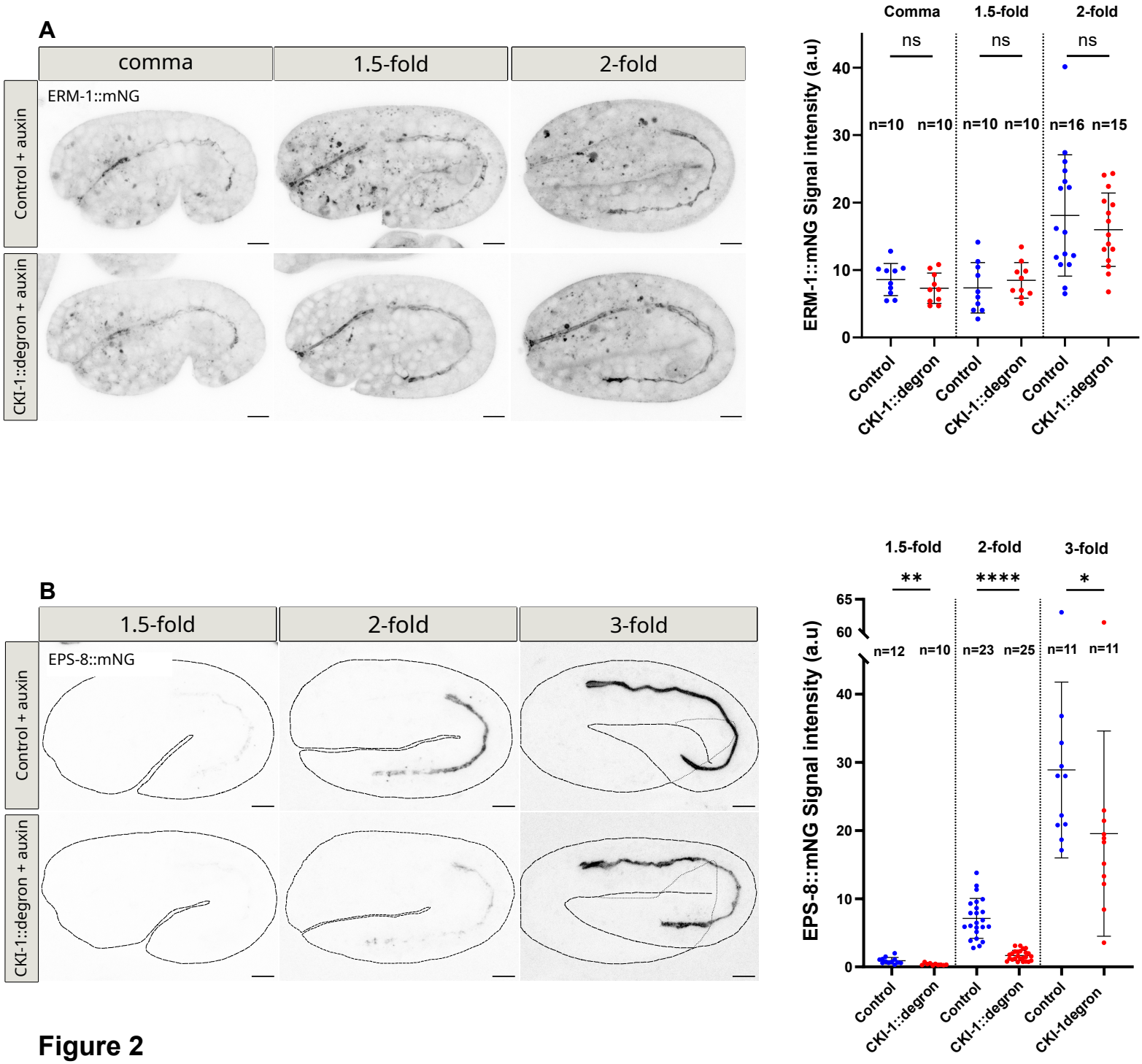
A
comma
1.5-fold
2-fold
ERM-1::mNG
Control + auxin
CKI-1::degron + auxin
Comma
1.5-fold
2-fold
ns
ns
ns
n=10
n=10
n=10
n=10
n=16
n=15
ERM-1::mNG Signal intensity (a.u)
0
10
20
30
40
Control
CKI-1::degron
Control
CKI-1::degron
Control
CKI-1::degron
B
1.5-fold
2-fold
3-fold
EPS-8::mNG
Control + auxin
CKI-1::degron + auxin
1.5-fold
2-fold
3-fold
**
****
*
n=12
n=10
n=23
n=25
n=11
n=11
EPS-8::mNG Signal intensity (a.u)
0
10
20
30
40
60
65
Control
CKI-1::degron
Control
CKI-1::degron
Control
CKI-1degron

Figure 2

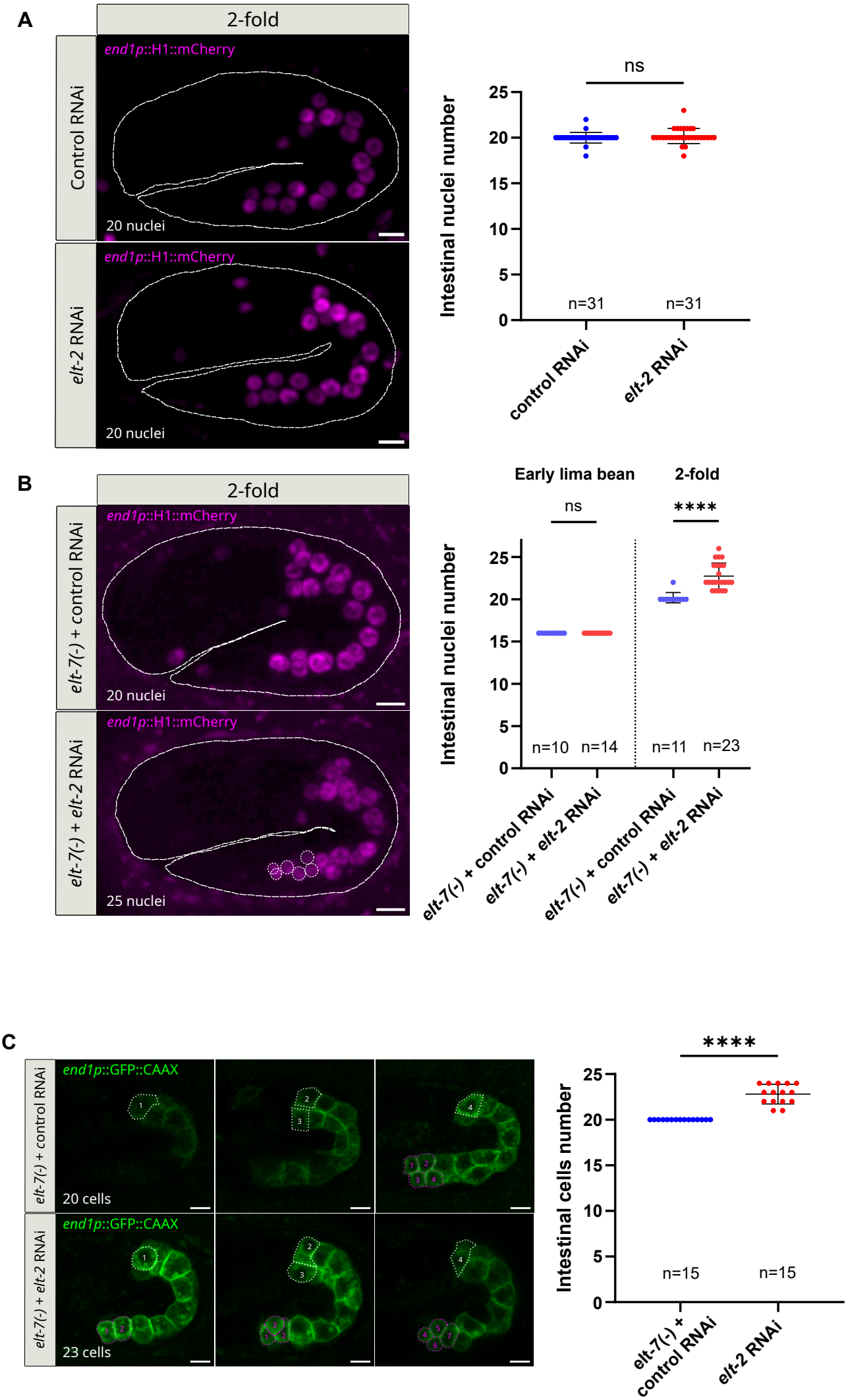
A
2-fold
Control RNAi
end1p::H1::mCherry
20 nuclei
elt-2 RNAi
end1p::H1::mCherry
20 nuclei
ns
Intestinal nuclei number
25
20
15
10
5
0
n=31
n=31
control RNAi
elt-2 RNAi
B
2-fold
elt-7(-) + control RNAi
end1p::H1::mCherry
20 nuclei
elt-7(-) + elt-2 RNAi
end1p::H1::mCherry
25 nuclei
Early lima bean
2-fold
ns
****
Intestinal nuclei number
n=10
n=14
n=11
n=23
elt-7(-) + control RNAi
elt-7(-) + elt-2 RNAi
elt-7(-) + control RNAi
elt-7(-) + elt-2 RNAi
C
elt-7(-) + control RNAi
end1p::GFP::CAAX
20 cells
elt-7(-) + elt-2 RNAi
end1p::GFP::CAAX
23 cells
****
Intestinal cells number
n=15
n=15
elt-7(-) + control RNAi
elt-2 RNAi

Figure 3

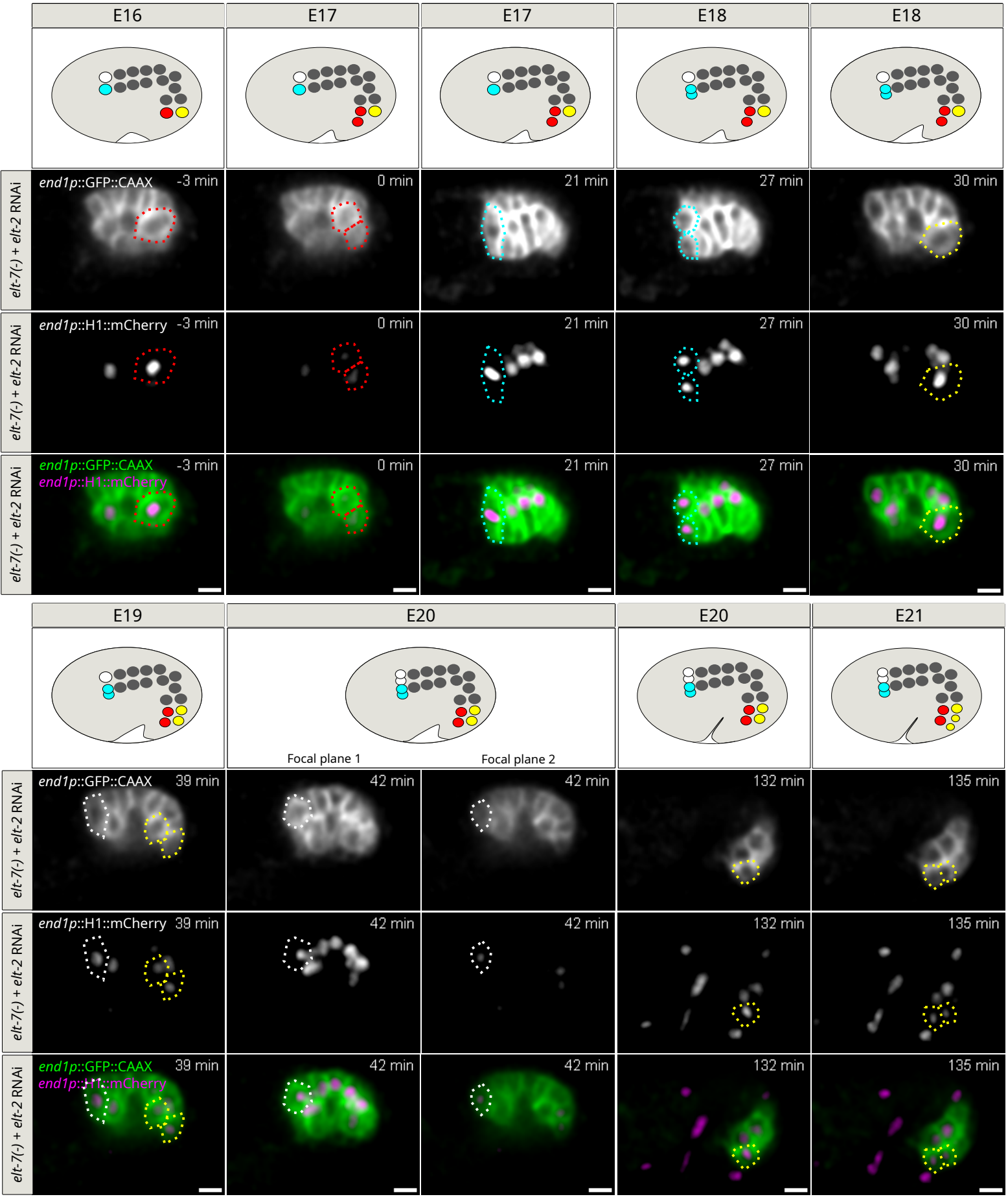
E16
E17
E17
E18
E18
elt-7(-) + elt-2 RNAi
end1p::GFP::CAAX
-3 min
0 min
21 min
27 min
30 min
end1p::H1::mCherry
end1p::GFP::CAAX
end1p::H1::mCherry
E19
E20
E20
E21
Focal plane 1
Focal plane 2
39 min
42 min
132 min
135 min

Figure 4

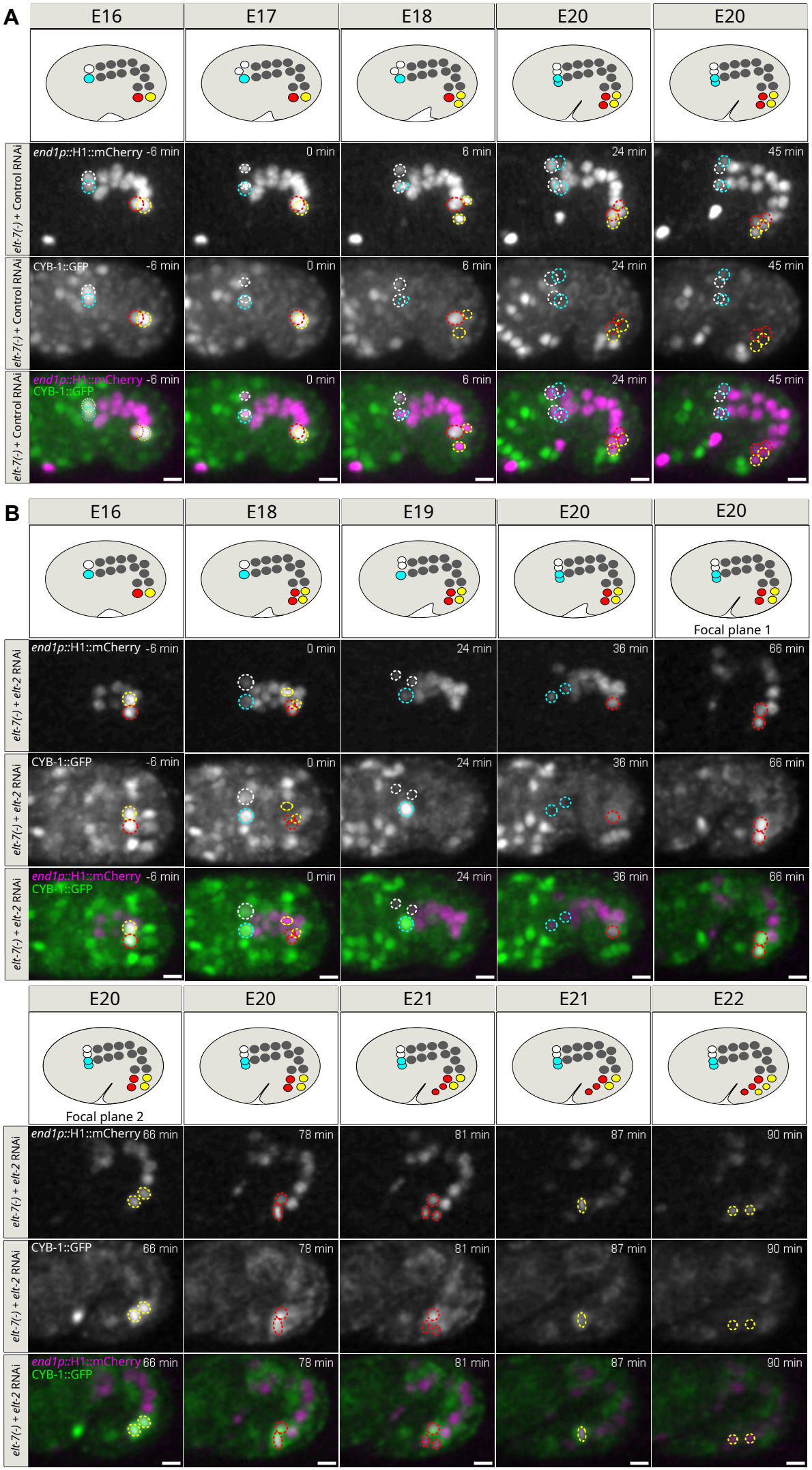
A
E16
E17
E18
E20
E20
elt-7(-) + Control RNAi
end1p::H1::mCherry -6 min
0 min
6 min
24 min
45 min
CYB-1::GFP
end1p::H1::mCherry
CYB-1::GFP
B
E16
E18
E19
E20
E20
Focal plane 1
elt-7(-) + elt-2 RNAi
36 min
66 min
E20
E20
E21
E21
E22
Focal plane 2
78 min
81 min
87 min
90 min

Figure 5

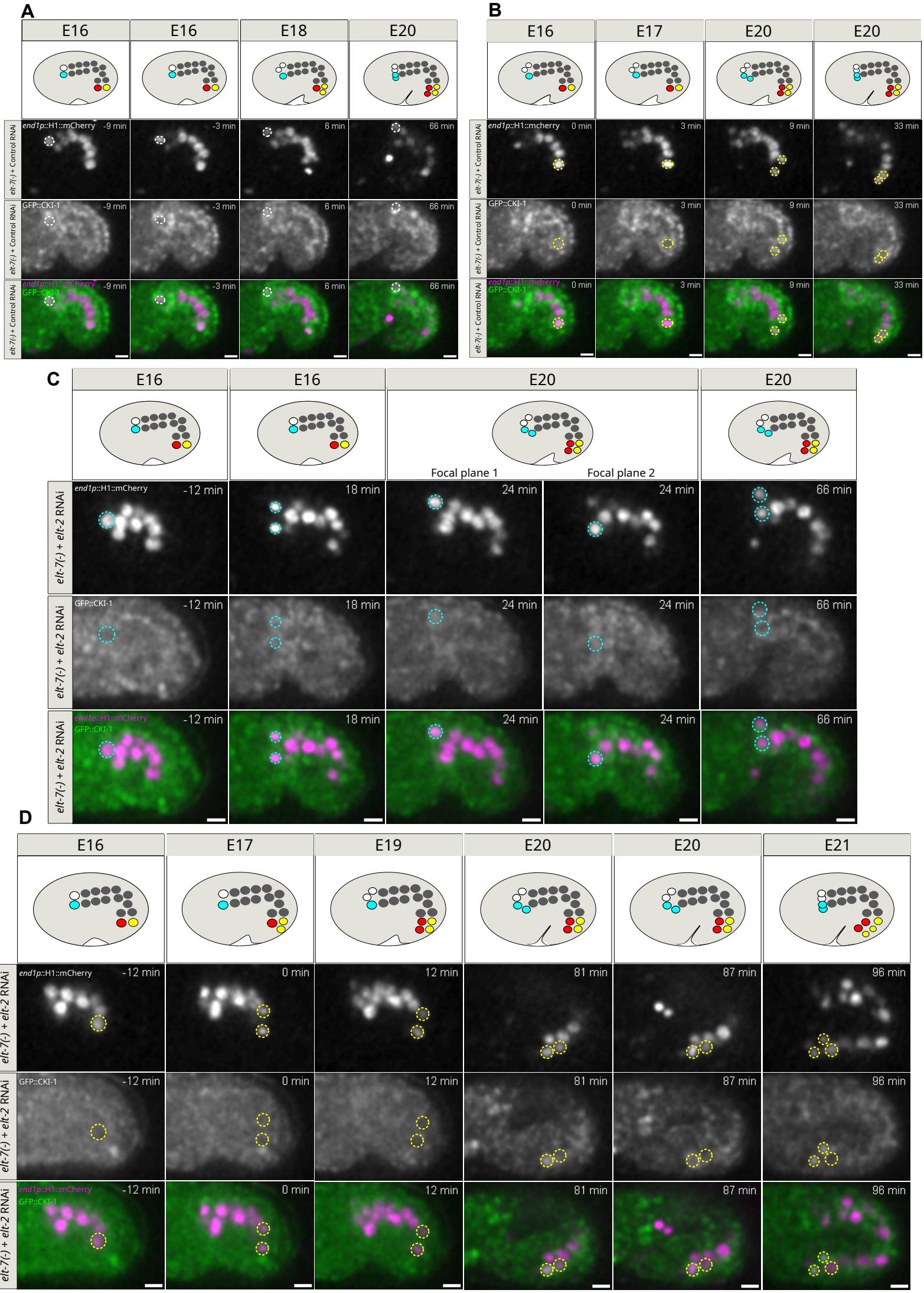
A
E16
E16
E18
E20
end1p::H1::mCherry
-9 min
-3 min
6 min
66 min
elt-7(-) + Control RNAi
GFP::CKI-1
end1p::H1::mCherry
GFP::CKI-1
B
E16
E17
E20
E20
end1p::H1::mcherry
0 min
3 min
9 min
33 min
C
E16
E16
E20
E20
Focal plane 1
Focal plane 2
elt-7(-) + elt-2 RNAi
-12 min
18 min
24 min
66 min
D
E16
E17
E19
E20
E20
E21
0 min
12 min
81 min
87 min
96 min

Figure 6

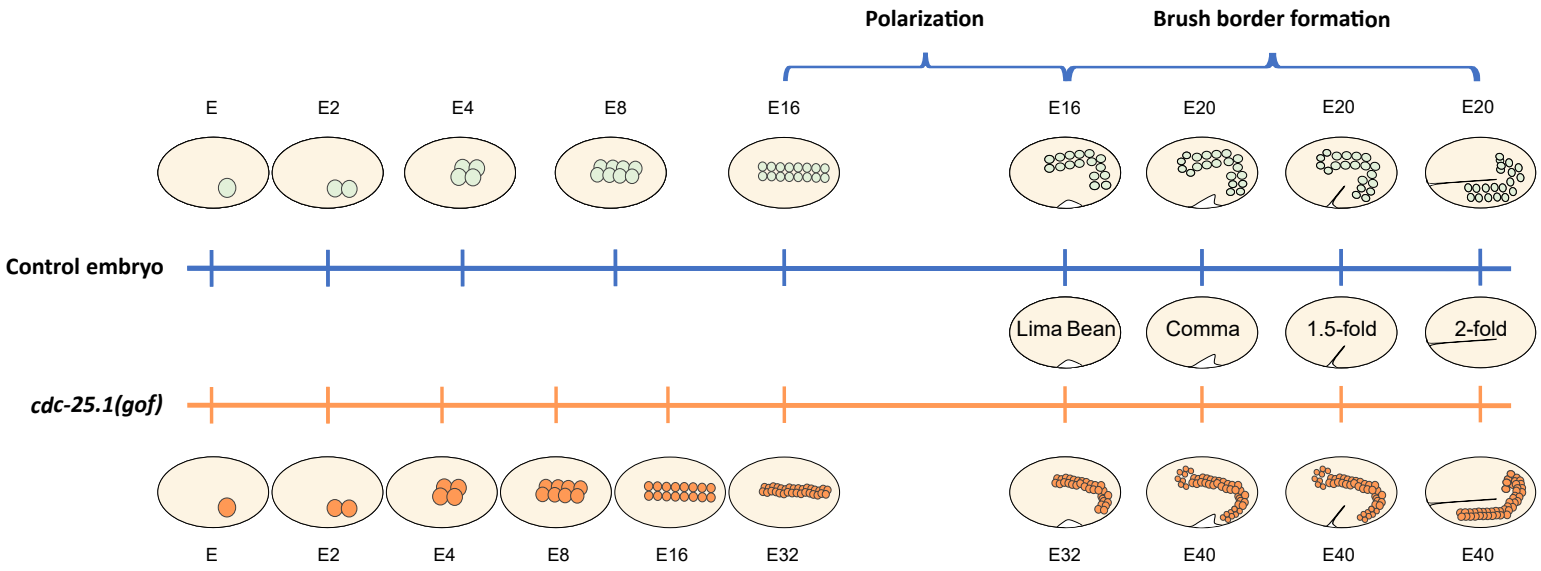
Polarization
Brush border formation
E
E2
E4
E8
E16
E16
E20
E20
E20
Control embryo
Lima Bean
Comma
1.5-fold
2-fold
cdc-25.1(gof)
E
E2
E4
E8
E16
E32
E32
E40
E40
E40

Figure S1

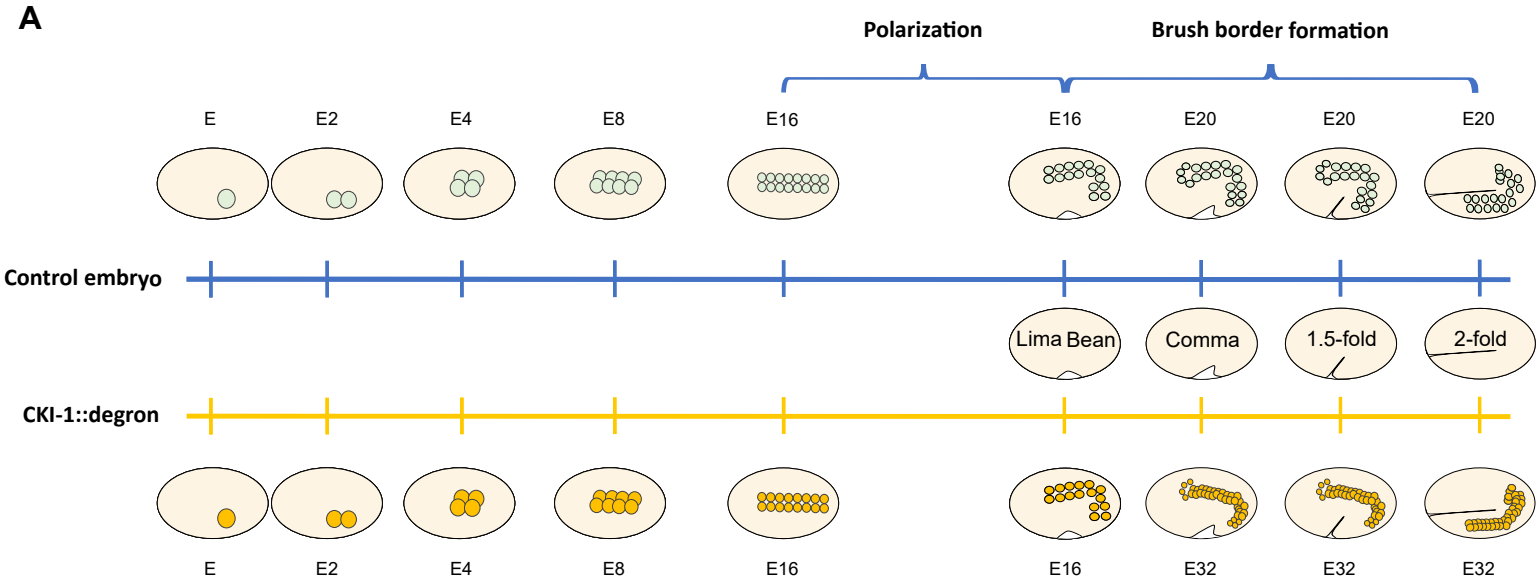
A
Polarization
Brush border formation
E
E2
E4
E8
E16
E16
E20
E20
E20
Control embryo
Lima Bean
Comma
1.5-fold
2-fold
CKI-1::degron
E
E2
E4
E8
E16
E16
E32
E32
E32

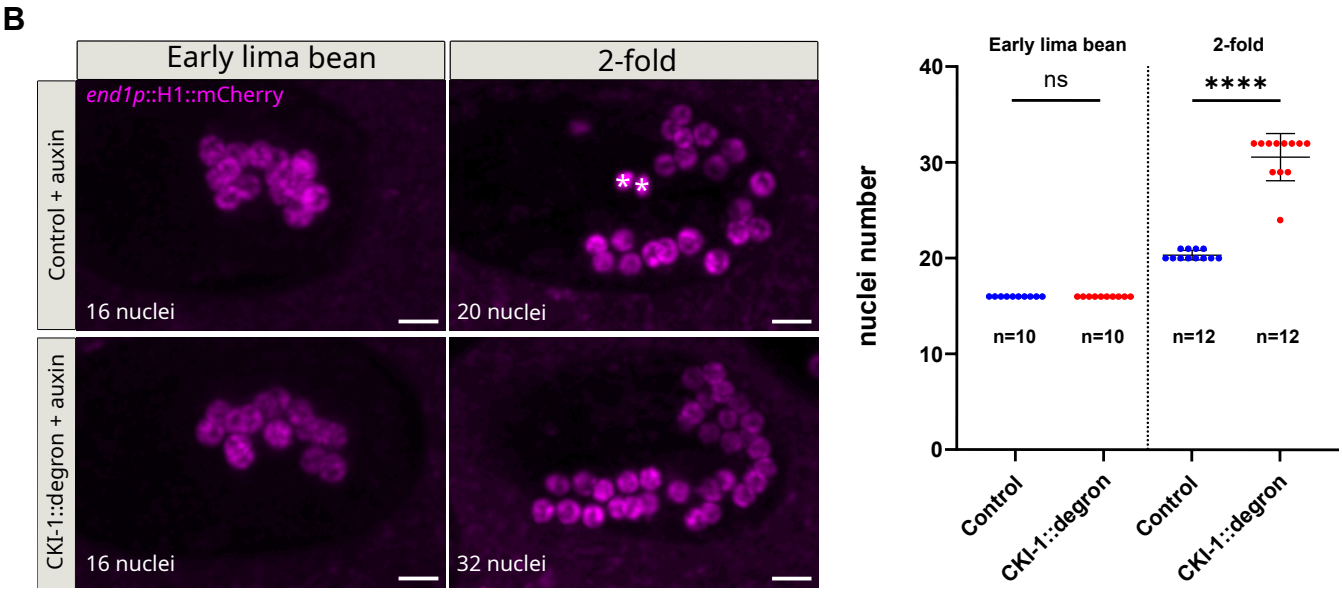
B
Early lima bean
2-fold
end1p::H1::mCherry
Control + auxin
CKI-1::degron + auxin
16 nuclei
20 nuclei
16 nuclei
32 nuclei
Early lima bean
2-fold
ns
****
nuclei number
40
30
20
10
0
n=10
n=10
n=12
n=12
Control
CKI-1::degron
Control
CKI-1::degron

Figure S2

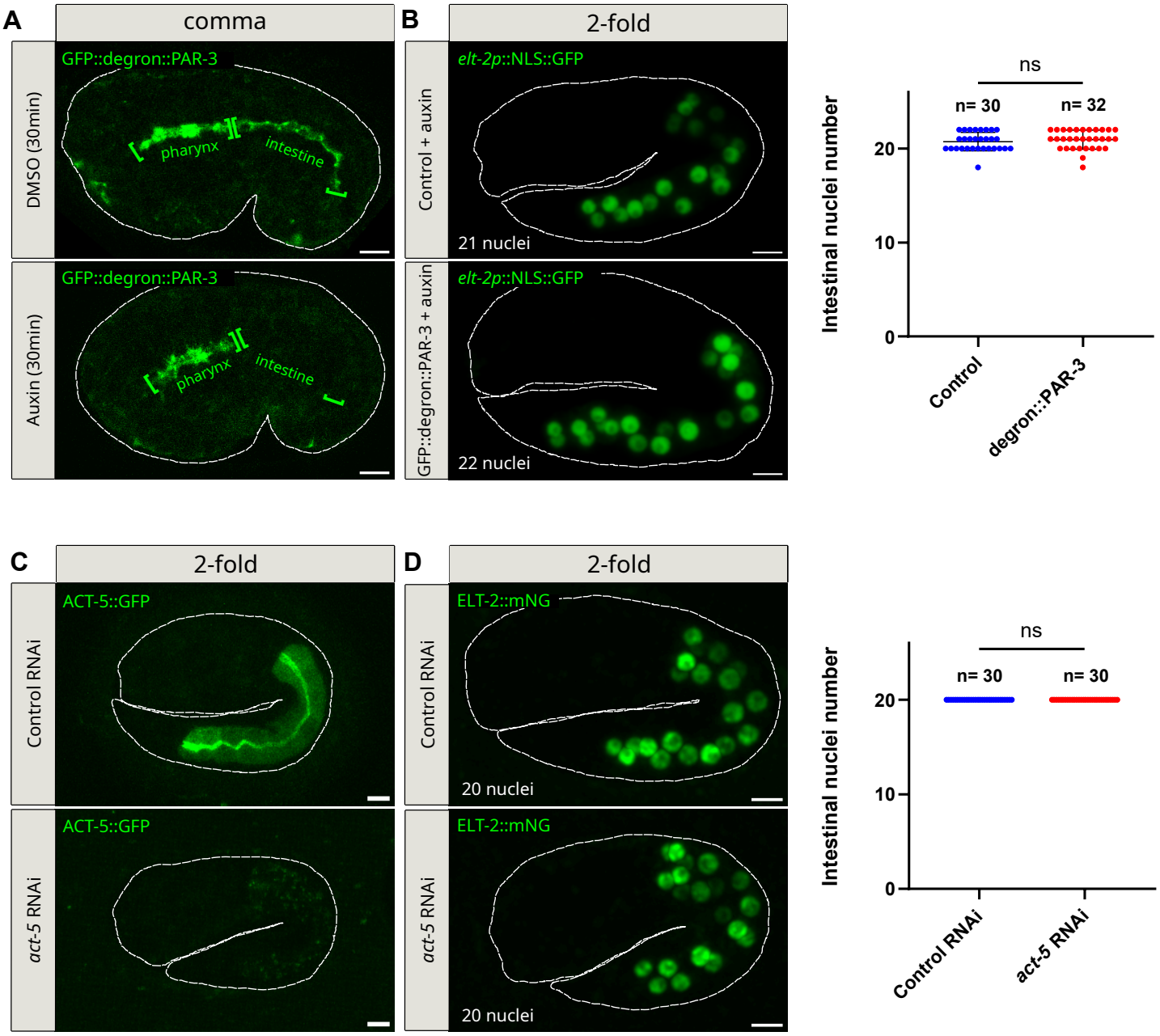
A
comma
DMSO (30min)
GFP::degron::PAR-3
pharynx
intestine
Auxin (30min)
GFP::degron::PAR-3
pharynx
intestine
B
2-fold
Control + auxin
elt-2p::NLS::GFP
21 nuclei
GFP::degron::PAR-3 + auxin
elt-2p::NLS::GFP
22 nuclei
ns
n= 30
n= 32
Intestinal nuclei number
20
10
0
Control
degron::PAR-3
C
2-fold
Control RNAi
ACT-5::GFP
act-5 RNAi
ACT-5::GFP
D
2-fold
Control RNAi
ELT-2::mNG
20 nuclei
act-5 RNAi
ELT-2::mNG
20 nuclei
ns
n= 30
n= 30
Intestinal nuclei number
20
10
0
Control RNAi
act-5 RNAi

Figure S3

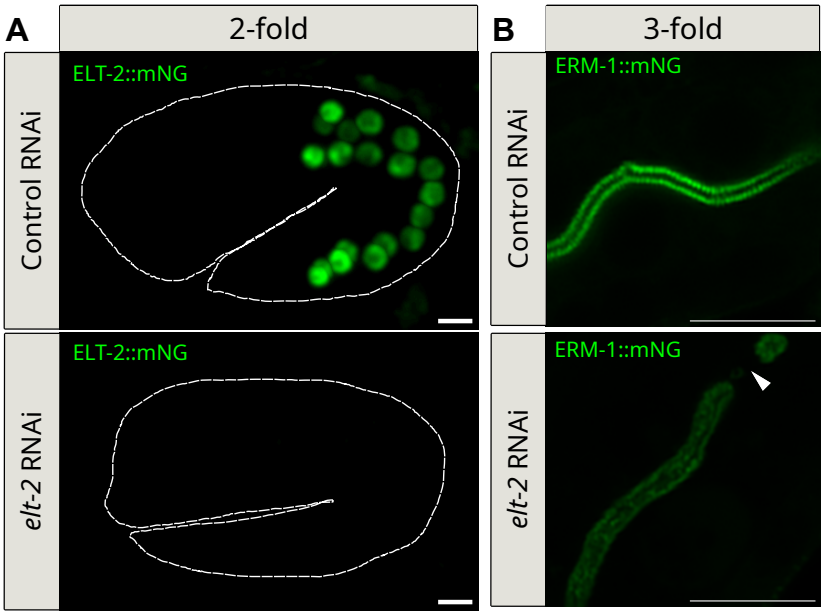
A
2-fold
B
3-fold
Control RNAi
ELT-2::mNG
ERM-1::mNG
elt-2 RNAi
ELT-2::mNG
ERM-1::mNG

Figure S4

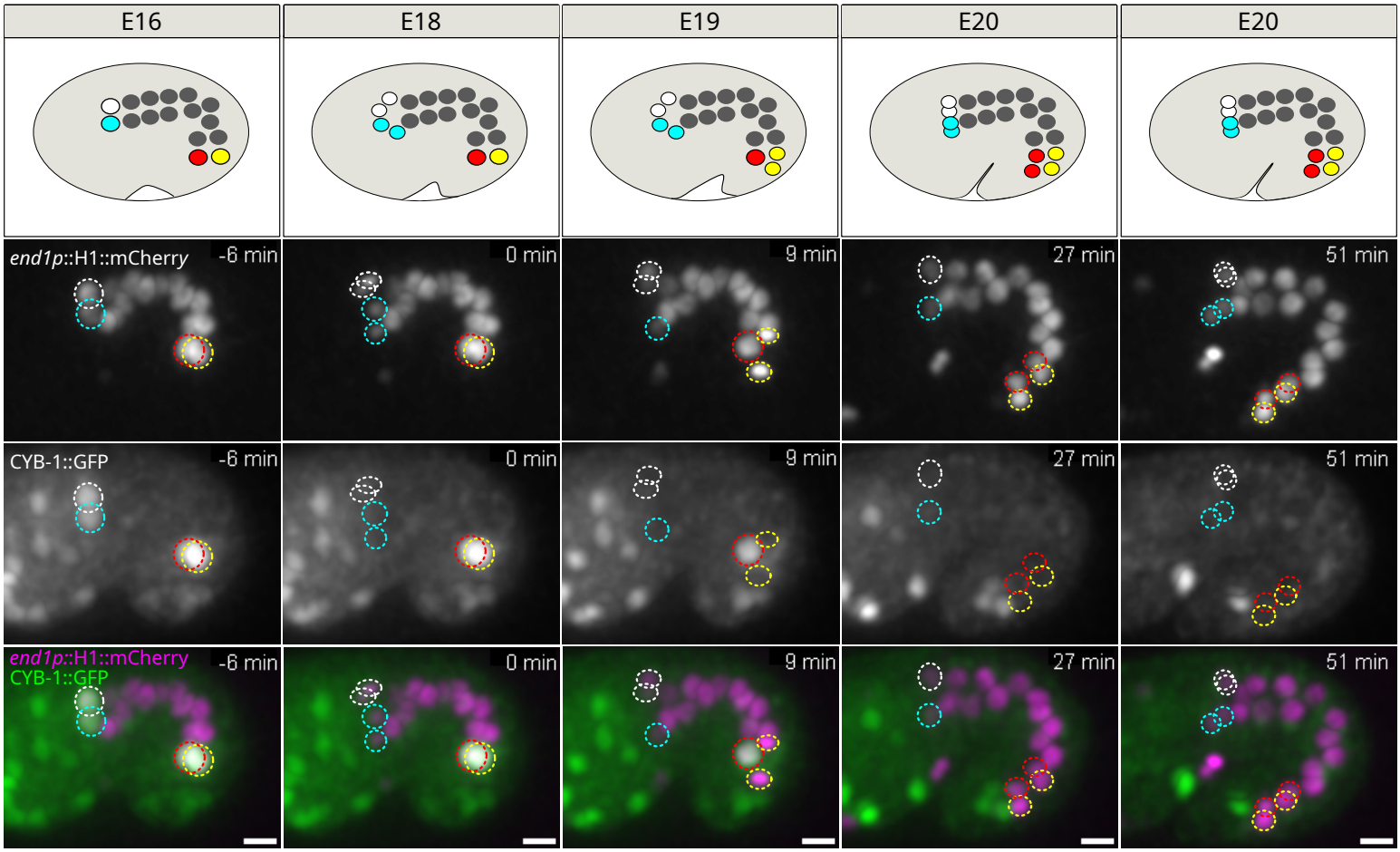
E16
E18
E19
E20
E20
end1p::H1::mCherry
CYB-1::GFP
end1p::H1::mCherry
CYB-1::GFP
-6 min
0 min
9 min
27 min
51 min

Figure S5

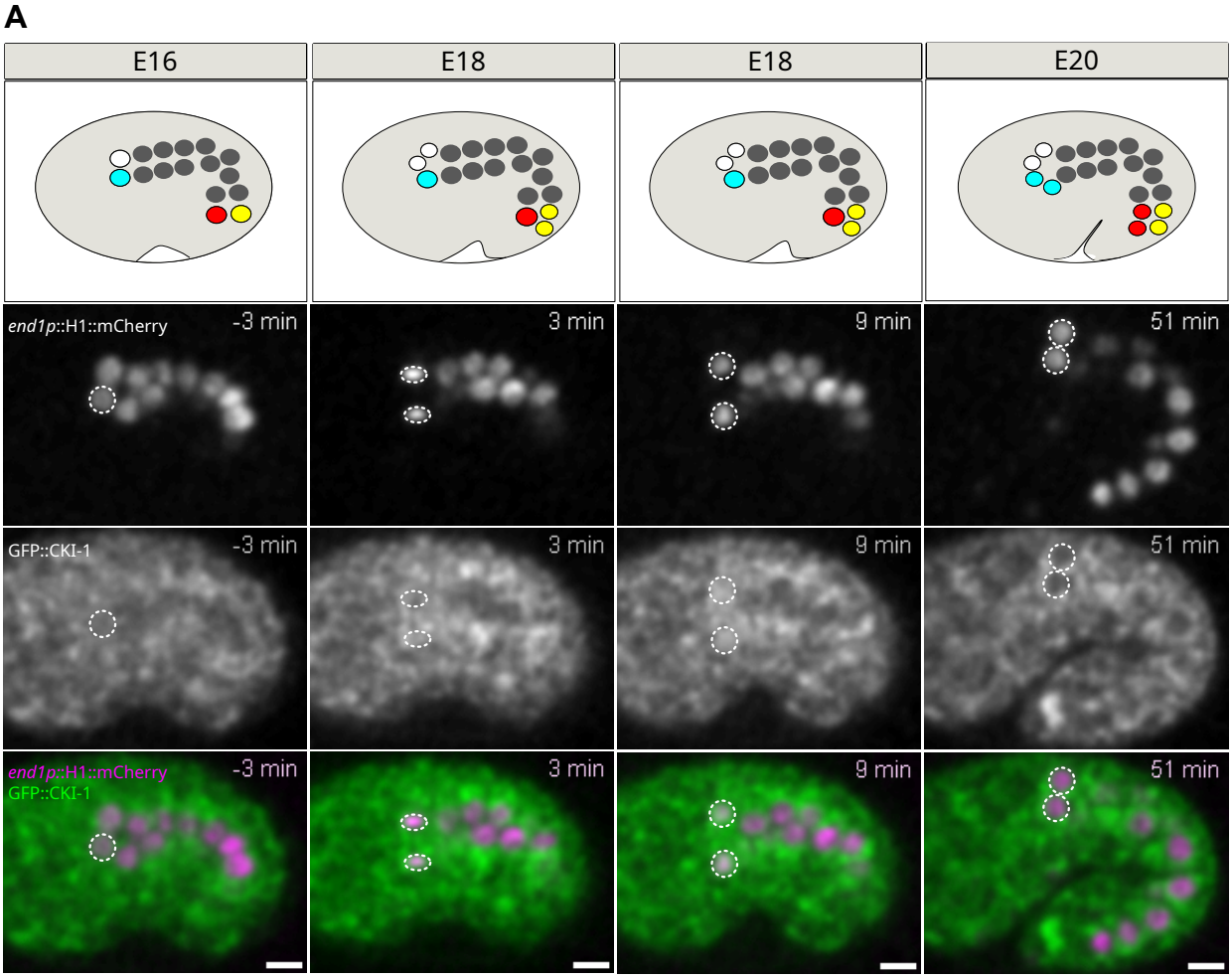
A
E16
E18
E18
E20
end1p::H1::mCherry
-3 min
3 min
9 min
51 min
GFP::CKI-1
-3 min
3 min
9 min
51 min
end1p::H1::mCherry
GFP::CKI-1
-3 min
3 min
9 min
51 min

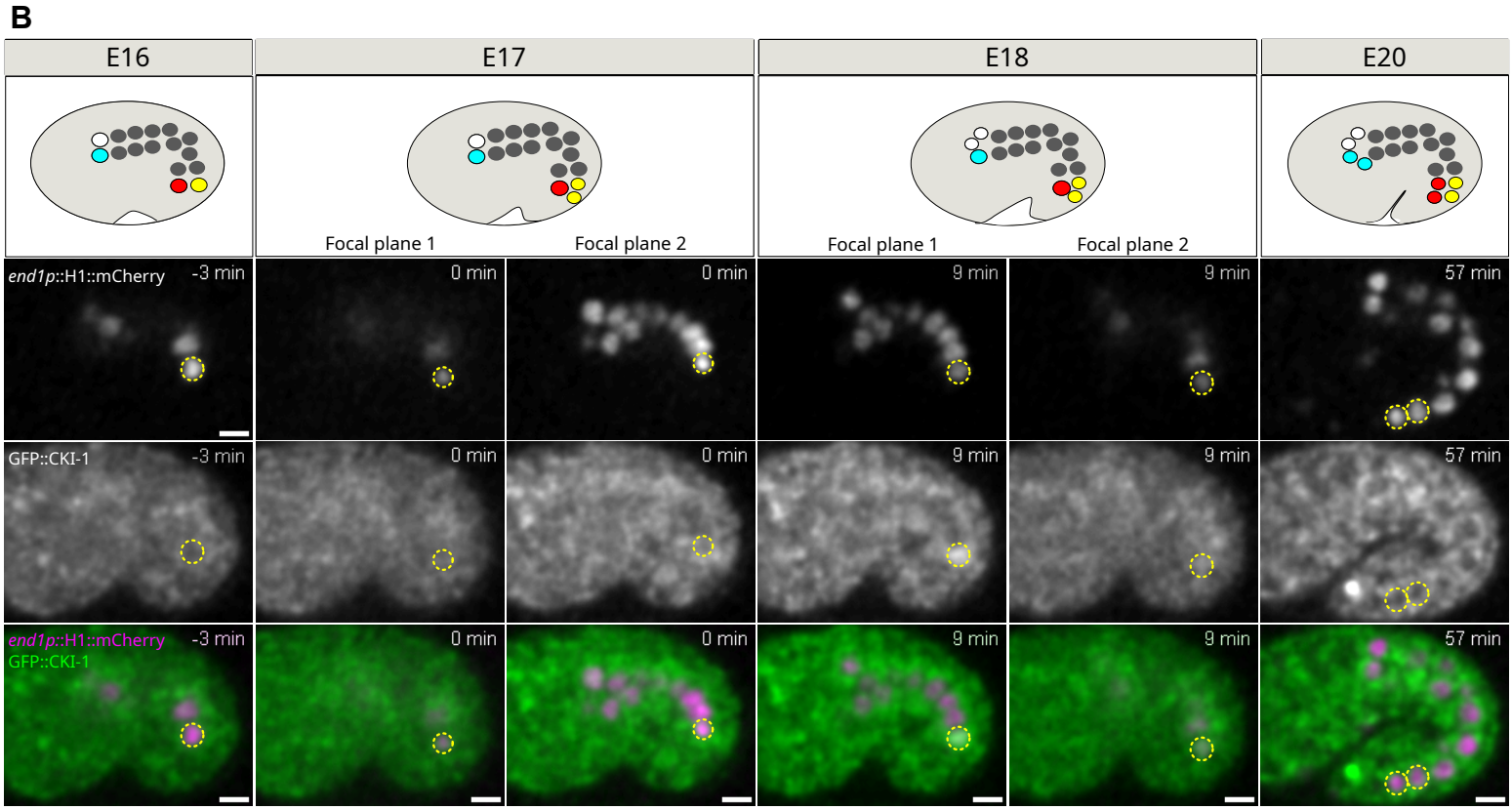
B
E16
E17
E18
E20
Focal plane 1
Focal plane 2
Focal plane 1
Focal plane 2
end1p::H1::mCherry
-3 min
0 min
0 min
9 min
9 min
57 min
GFP::CKI-1
-3 min
0 min
0 min
9 min
9 min
57 min
end1p::H1::mCherry
GFP::CKI-1
-3 min
0 min
0 min
9 min
9 min
57 min

Figure S6

Table S1: *C. elegans* strains used in this study

Strain	Complete genotype	Source	Figures
FL676	*cdc-25.1(rr31) hmr-1(cp57[hmr-1::mKate2]) I; par-3(it298[par-3::gfp]) III; stIs10220[end-1p::his-24::mCherry::let-858 3' UTR + unc-119(+)]*	This study *hmr-1(cp57)* from OX704 (Soto lab (Sasidharan et al., 2018); originally from LP238, Goldstein lab) *par-3(it298)* from KK1216 (Kemphues lab) *stIs10220* from RW10234 (Waterston lab, via CGC)	Fig.1A
FL677	*hmr-1(cp57[hmr-1::mKate2]) I; par-3(it298[par-3::gfp]) III; stIs10220[end-1p::his-24::mCherry::let-858 3' UTR + unc-119(+)]*	This study	Fig.1A
FL678	*erm-1(bab59[erm-1::mNG^3xFlag]) cdc-25.1(rr31) hmr-1(cp57[hmr-1::mKate2]) I; stIs10220[end-1p::his-24::mCherry::let-858 3' UTR + unc-119(+)]*	This study *erm-1(bab59)* from FL378 (Bidaud-Meynard et al., 2019)	Fig.1B
FL697	*erm-1(bab59[erm-1::mNG^3xFlag]) I, hmr-1(cp57[hmr-1::mKate2]) I; stIs10220[end-1p::his-24::mCherry::let-858 3' UTR + unc-119(+)]*	This study	Fig.1B
FL644	*cdc-25.1(rr31) I, hmr-1(cp57[hmr-1::mKate2]) I; eps-8(bab140[eps-8::mNG]) IV*	This study *eps-8(bab140)* from FL290 (Bidaud-Meynard et al., 2021)	Fig.1C
FL552	*hmr-1(cp57[hmr-1::mKate2]) I; eps-8(bab140[eps-8::mNG]) IV*	This study	Fig.1C
FL748	*erm-1(bab59[erm-1::mNG^3xFlag]) I; mibIs48[elt-2p::TIR-1::tagBFP2-Lox511::tbb-2-3'UTR, IV:5014740-5014802(cxTi10882 site)] IV; stIs10220[end-1p::his-24::mCherry::let-858 3' UTR + unc-119(+)]*	This study *mibIs48* from BOX273 (Boxem lab (Castiglioni et al., 2020)	Fig.2A
FL763	*erm-1(bab59[erm-1::mNG^3xFlag]) I; cki-1(bab393[cki-1::AID::tagBFP2]) II; mibIs48[elt-2p::TIR-1::tagBFP2-Lox511::tbb-2-3'UTR, IV:5014740-5014802(cxTi10882 site)] IV; stIs10220[end-1p::his-24::mCherry::let-858 3' UTR + unc-119(+)*	This study *cki-1(bab393)* from FL733 (this study)	Fig.2A
FL755	*eps-8(bab140[eps-8::mNG]) mibIs48[elt-2p::TIR-1::tagBFP2-Lox511::tbb-2-3'UTR, IV:5014740-5014802(cxTi10882 site)] IV; stIs10220[end-1p::his-24::mCherry::let-858 3' UTR + unc-119(+)]*	This study	Fig.2B
FL764	*cki-1(bab393[cki-1::AID::tagBFP2]) II; eps-8(bab140[eps-8::mNG]) IV mibIs48[elt-2p::TIR-1::tagBFP2-Lox511::tbb-2-3'UTR, IV:5014740-5014802(cxTi10882 site)] IV; stIs10220[end-1p::his-24::mCherry::let-858 3' UTR + unc-119(+)]*	This study	Fig.2B
FL630	*stIs10220[end-1p::his-24::mCherry::let-858 3' UTR + unc-119(+)]*	This study	Fig.3A
FL734	*elt-7(tm840) V; stIs10220[end-1p::his-24::mCherry::let-858 3' UTR + unc-119(+)]*	This study *elt-7(tm840)* from MS433 (Mitani lab, via Maduro lab, (McGhee et al., 2007))	Fig.3B

FL747	*elt-7(tm840) zuIs70[end-1p::GFP::CAAX] V; stIs10220[end-1p::his-24::mCherry::let-858 3' UTR + unc-119(+)]*	This study *zuIs70* from MS2293 (Maduro lab (Choi et al., 2017), originally from Nance lab (Wehman et al., 2011))	Fig.3C Fig.4
FL760	*cyb-1(tn1806[cyb-1::GFP::tev::3xflag]) IV; elt-7(tm840) V; stIs10220[end-1p::his-24::mCherry::let-858 3' UTR + unc-119(+)]*	This study *cyb-1(tn1806)* from DG4569 (Greenstein lab, via CGC (Spike et al., 2022))	Fig.5
FL758	*cki-1(bmd132[GFP::LoxP::cki-1::3xFLAG]) II; elt-7(tm840) V; stIs10220[end-1p::his-24::mCherry::let-858 3' UTR + unc-119(+)]*	This study *cki-1(bmd132)* from DQM455 (Matus lab, via CGC (Adikes et al., 2020))	Fig.6
FL741	*mibIs48[elt-2p::TIR-1::tagBFP2-Lox511::tbb-2-3'UTR, IV:5014740-5014802(cxTi10882 site)] IV; stIs10220[end-1p::his-24::mCherry::let-858 3' UTR + unc-119(+)]*	This study	Fig.S2B
FL753	*cki-1(bab393[cki-1::AID::tagBFP2]) II; mibIs48[elt-2p::TIR-1::tagBFP2-Lox511::tbb-2-3'UTR, IV:5014740-5014802(cxTi10882 site)] IV; stIs10220[end-1p::his-24::mCherry::let-858 3' UTR + unc-119(+)]*	This study	Fig.S2B
FL511	*par-3(mib68[eGFP-Lox2272::aid::par-3b+eGFP(noIntrons)-LoxP::aid::par-3g]) III; mibIs48[elt-2p::TIR-1::tagBFP2-Lox511::tbb-2-3'UTR, IV:5014740-5014802(cxTi10882 site)] IV*	This study *par-3(mib68)* from BOX290 (Boxem lab (Castiglioni et al., 2020)	Fig.S3A
FL605	*hmr-1(cp57[hmr-1::mKate2]) I; par-3(mib68[eGFP-Lox2272::aid::par-3b+eGFP(noIntrons)-LoxP::aid::par-3g]) III; mibIs48[elt-2p::TIR-1::tagBFP2-Lox511::tbb-2-3'UTR, IV:5014740-5014802(cxTi10882 site)] IV; rrIs1[elt-2p::NLS::GFP::LacZ::unc-54 3'UTR + unc-119(+)] X*	This study *rrIs1* from MR142 (Roy lab, via CGC (Kostić and Roy, 2002)	Fig.S3B
FL607	*hmr-1(cp57[hmr-1::mKate2]) I; mibIs48[elt-2p::TIR-1::tagBFP2-Lox511::tbb-2-3'UTR, IV:5014740-5014802(cxTi10882 site)] IV; rrIs1[elt-2p::NLS::GFP::LacZ::unc-54 3'UTR + unc-119(+)] X*	This study	Fig.S3B
VJ268	*fgEx12[act-5p::act-5::GFP + unc-119(+)] II; unc-119(ed3) III*	Gobel lab (Zhang et al., 2012)	Fig.S3C
FL660	*elt-2(bab354[elt-2::mNG]) X*	(Demouchy et al., 2024)	Fig.S3D Fig.S4A
FL378	*erm-1(bab59[erm-1::mNG^3xFlag]) I*	(Bidaud-Meynard et al., 2019)	Fig.S4B
FL752	*cyb-1(tn1806[cyb-1::GFP::tev::3xflag]) IV; stIs10220[end-1p::his-24::mCherry::let-858 3' UTR + unc-119(+)]*	This study	Fig.S5
FL709	*cki-1(bmd132[GFP::LoxP::cki-1::3xFLAG]) II; stIs10220[end-1p::his-24::mCherry::let-858 3' UTR + unc-119(+)]*	This study	Fig.S6